# EDGEWOOD

CHEMICAL BIOLOGICAL CENTER

U.S. ARMY SOLDIER AND BIOLOGICAL CHEMICAL COMMAND

**ECBC-CR-062**

# FIELD-DEPLOYABLE CHEMICAL POINT DETECTION NETWORK

**Charles Pennington**

**Luna Innovations**
**Blacksburg, VA 24060**

**October 2003**

20040113 253

Aberdeen Proving Ground, MD 21010-5424

## DISCLAIMER

The findings in this report are not to be construed as an official Department of the Army position unless so designated by other authorizing documents.

| REPORT DOCUMENTATION PAGE | | | Form Approved<br>OMB No. 0704-0188 |
|---|---|---|---|

Public reporting burden for this collection of information is estimated to average 1 hour per response, including the time for reviewing instructions, searching existing data sources, gathering and maintaining the data needed, and completing and reviewing the collection of information. Send comments regarding this burden estimate or any other aspect of this collection of information, including suggestions for reducing this burden, to Washington Headquarters Services, Directorate for Information Operations and Reports, 1215 Jefferson Davis Highway, Suite 1204, Arlington, VA 22202-4302, and to the Office of Management and Budget, Paperwork Reduction Project (0704-0188), Washington, DC 20503.

| 1. AGENCY USE ONLY *(Leave Blank)* | 2. REPORT DATE<br>2003 October | 3. REPORT TYPE AND DATES COVERED<br>Final; 01 Mar – 03 Mar | |
|---|---|---|---|
| 4. TITLE AND SUBTITLE<br>Field-Deployable Chemical Point Detection Network | | | 5. FUNDING NUMBERS<br><br>C-DAAD13-01-C-0016 |
| 6. AUTHOR (S)<br>Pennington, Charles | | | |
| 7. PERFORMING ORGANIZATION NAME (S) AND ADDRESS (ES)<br>Luna Innovations, 2851 Commerce Street, Blacksburg, VA 24060 | | | 8. PERFORMING ORGANIZATION REPORT NUMBER<br><br>ECBC-CR-062 |
| 9. SPONSORING/MONITORING AGENCY NAME (S) AND ADDRESS (ES)<br>DIR, ECBC, ATTN: AMSRD-ECB-RT-II, APG, MD 21010-5424 | | | 10. SPONSORING/MONITORING AGENCY REPORT NUMBER |
| 11. SUPPLEMENTARY NOTES | | | |
| 12a. DISTRIBUTION/AVAILABILITY STATEMENT<br>Approved for public release; distribution is unlimited. | | | 12b. DISTRIBUTION CODE |

13. ABSTRACT (Maximum 200 words)

The probability of U.S. forces encountering CB agents during worldwide conflicts remains high. In the next 10 years, the threat from the proliferation of CBW weapons will increase. This will result from development of CB agents more difficult to detect and from adoption of more capable delivery systems. Several countries have CW capabilities (e.g., North Korea, China, India, Pakistan, Iran, Iraq, Syria, Libra, and the Independent States of the Former Soviet Union). The Joint Service Chemical and Biological Defense (CBD) Overview for FY00-FY01 identified early warning as the key to avoiding CB agent contamination. Standoff and point detection means, combined with effective collective and individual protective systems, can mitigate, even preclude an effective CBW attack. The CBD annual report acknowledges several major technical challenges to CB defense, including minimization of false positive/negative alarms, "size, weight, and power reduction of detectors, power generation and consumption, development of integrated biological and chemical detection systems, and the fusion of sensor data with mapping, imagery, and other data." To address these challenges, Luna focused development efforts on critical areas previously identified, "system miniaturization, improved sensitivity and specificity, agent characterizations and range, decreased false alarm rate, and decreased operation/support costs."

| 14. SUBJECT TERMS | | | 15. NUMBER OF PAGES<br>49 |
|---|---|---|---|
| Long period grating<br>Chemical agents<br>Nerve agent | Blister agent<br>Networking<br>Detection | | |
| | | | 16. PRICE CODE |
| 17. SECURITY CLASSIFICATION OF REPORT<br>UNCLASSIFIED | 18. SECURITY CLASSIFICATION OF THIS PAGE<br>UNCLASSIFIED | 19. SECURITY CLASSIFICATION OF ABSTRACT<br>UNCLASSIFIED | 20. LIMITATION OF ABSTRACT<br>UL |

NSN 7540-01-280-5500

Standard Form 298 (Rev. 2-89)
Prescribed by ANSI Std. Z39-18
298-10

Blank

## PREFACE

The work described in this report was authorized under Contract No. DAAD13-01-C-0016. This work was started in March 2001 and completed in March 2003.

The use of either trade or manufacturers' names in this report does not constitute an official endorsement of any commercial products. This report may not be cited for purposes of advertisement.

This report has been approved for public release. Registered users should request additional copies from the Defense Technical Information Center; unregistered users should direct such request to the National Technical Information Service.

Blank

# CONTENTS

# FIGURES

## TABLES

Blank

# FIELD-DEPLOYABLE CHEMICAL POINT DETECTION NETWORK

1.     SIGNIFICANCE AND SUMMARY OF PROGRAM
       ACCOMPLISHMENTS

According to the 2000 Chemical and Biological Defense (CBD) Annual Report to Congress, "The probability of U.S. forces encountering CB agents during worldwide conflicts remains high . . . In the next 10 years, the threat from the proliferation of CBW weapons will certainly increase. This will result from the development of chemical and biological agents that are more difficult to detect and from the adoption of more capable delivery systems." Several countries have chemical warfare capability, including North Korea, China, India, Pakistan, Iran, Iraq, Syria, Libya, and the Independent States of the Former Soviet Union. [CBD, 2000] The Joint Service Chemical and Biological Defense Overview for FY00-FY01 identified early warning as the key to avoiding chemical and biological agent contamination. This report recognized that, "standoff and point detection means, combined with effective collective and individual protective systems, can mitigate, even preclude an effective CBW attack." [CBDP, 2000] The CBD Annual Report acknowledged several major technical challenges to chemical and biological defense including minimization of false positive and negative alarms, "size, weight, and power reduction of detectors, power generation and consumption, development of integrated biological and chemical detection systems, and the fusion of sensor data with mapping, imagery, and other data." [CBD, 2000] To address these challenges Luna focused development efforts on the critical areas that the Department of Defense has identified, "system miniaturization, improved sensitivity and specificity, agent characterizations and range, decreased false alarm rate, and decreased operation and support costs." [CBD, 2000]

During the proposed Phase II program, Luna Innovations integrated the technology demonstrated during the Phase I program into a complete detection system to meet the challenges of chemical defense. Luna has demonstrated battery-powered optical fiber support electronics with a wireless communication system and GPS capability, a fiber optic based biosensor utilizing reactive polymers to detect chemical agents, and an air sampling system that will concentrate the sample prior to exposure of the sensor if necessary. Highlights of the Phase II program can be seen in Figures 1 and 2. The detection of ethyl butyrate is demonstrated in Figure 2 by the use of organophosphate hydrolase (OPH) immobilized on a pH sensitive hydrogel coated LPG sensor. The data demonstrates the ability to measure the pH change during the hydrolysis reaction.

The field-deployable point detection network under development by Luna consists of a laptop-based central communication hub and several miniature agent detection units (MADUs). The MADU is comprised of wireless networked detector platforms utilizing reactive polymer coated fibers to detect chemical warfare agents. The system under development by Luna is highly multiplexed, reducing the possibility of false alarms. Luna also designed the system to be compatible with biological warfare (BW) detection systems under concurrent Department of Defense Phase II SBIR programs. The BW detection platform utilizes Luna's Long Period Grating technology and fluorescence for the orthogonal confirmation of the detection of BW agents. By combining the two detection technologies the probability of false detection of BW agents is reduced. The focus of this program was to develop a complete field deployable CB detection system that meets the Contamination Avoidance Defense Technology Objectives

9

of early warning, point detection, and reporting of chemical and biological attacks. The ability of the platforms to exist as nodal detection units deployed as monitors in suspected areas of engagement would provide the capability of plume detection in remote areas. Luna firmly believes this technology will provide a great improvement in chemical and biological warfare readiness of the U.S. military by improving the portability, networking, sampling time, reliability and sensitivity of current CB sensor systems such as the Joint Chemical Agent Detector (JCAD) or Portal Shield technology.
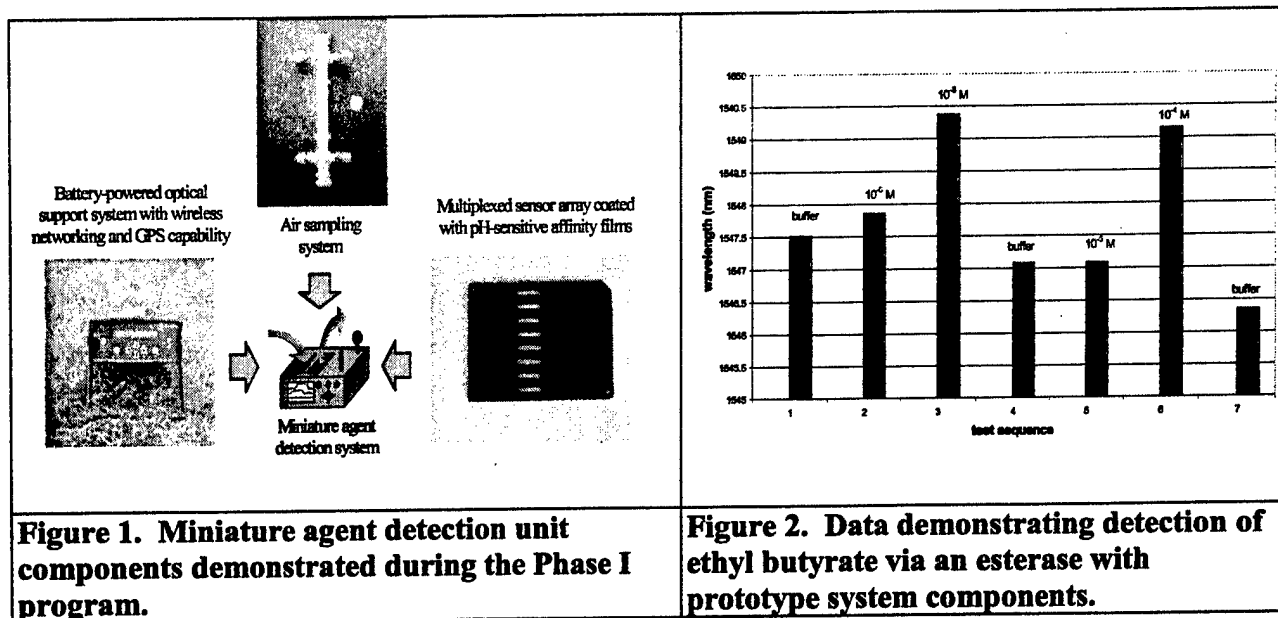


| Figure 1. Miniature agent detection unit components demonstrated during the Phase I program. | Figure 2. Data demonstrating detection of ethyl butyrate via an esterase with prototype system components. |

Luna's technology will greatly increase the US commanders' knowledge of the battle space through point detection of chemical agents. In addition to the direct threat to the life of the war fighter, chemical agents impact logistical planning of the battle space by limiting the full range of weapons available by denying access to weapons staging areas, blocking important entry points for munitions delivery, and targeting command and control nodes [CBDP 2000]. The units proposed by Luna will be distributed throughout the battle space and the MADU will continuously sample the air while monitoring for the presence of chemical agents. Status reports from the MADU will be continuously sent to either a local system hub at a mobile command center within the battle space, or via a satellite link to a central command center. Information from the MADU will include position (from the GPS) and chemical agent concentration measurements, which can then be used by US commanders to manage the battle space for precision engagement with minimal risk to the war fighter and maximum tactical advantage.

## 2. TECHNICAL OBJECTIVES

The objective of the proposed Phase II program was to build upon the success of the Phase I effort and produce a commercially viable, field-deployable miniature system for the detection of chemical warfare agents including nerve and blister. One of the goals of the Phase II program

was to develop a reliable detection system with minimal false alarms, and enough sensitivity to positively detect the agent. Sensors with no polymer coating (control sensors) were used to reduce the incidence of false alarms. Any response with the control sensor is due to non-specific environmental conditions and the responses from these sensors are nulled from the responses from the polymer-coated sensors. Several key components that form the basis for the Phase II technical objectives are listed below.

**Task 1. Optimize the pH sensitive hydrogel coating.** New pH sensitive hydrogel coatings will be developed and optimized to provide increased sensitivity to pH changes and produce a rugged coating. In Phase I, the primary target was a simulant for the organophosphate nerve agents. During the Phase II, program the detection menu was expanded to include the detection of blister agents. The use of control sensors was implemented to reduce the rate of false detection.

**Task 2. Miniaturize subcomponents.** Subcomponents were developed to reduce the overall size of the system. Specific areas of miniaturization included the signal processing electronics, spectrometer, and packaging.

**Task 3. Develop air-sampling system.** Luna finalized the development and integration of the fiber optic system with the air sampling technology provided by MesoSystems Technology. The development focused on a compact sampling system that delivered a vapor phase sample.

**Task 4. Integrate subcomponents.** The individual subcomponents for wireless communication, GPS location, and signal demodulation, were integrated into a single miniature unit. The air sampling system and sensor were integrated into a single unit that is interfaced to the electronics unit.

**Task 5. Test integrated system with simulants and interferrents.** Multiplexed sensor arrays were fabricated with redundancy to provide statistical analysis of false positive rates. A true positive result would require all sensors to respond to a sample; if only one of the sensors responds, there is a high probability that it is a false positive. The sensors could be coated with various coatings that respond differently to chemical warfare agents, thereby creating a matrix of responses based upon the agent. Samples consisted of known simulants for chemical warfare agents.

**Task 6. Establish commercialization plan.** Throughout the Phase II efforts, Luna performed market analysis within the proteomics industry where the unique characteristics of a rapid, portable, highly sensitive, quantitative and specific sensor provide a definitive competitive advantage. Likewise, the sensing technology developed under this contract was used to aid in the spin-off of Luna Analytics and Luna Energy for the commercialization of the LPG sensing platform.

11

## 3. TECHNICAL BACKGROUND AND APPROACH

The principle behind the LPG sensor is that Germania doped fused-silica glass is photosensitive such that fiber exposure to certain wavelengths of light, particularly 244 nm, will cause the refractive index of the glass to increase slightly [Hill, 1978]. If the fiber is exposed to a periodic index variation, the refractive index of the optical fiber is modulated forming a structure analogous to the Bragg gratings formed by crystal lattices. This grating, based on its periodicity, will selectively reflect wavelengths. Figure 3 provides a schematic of a long-period optical fiber grating and shows how it interacts with light propagating in the fiber.
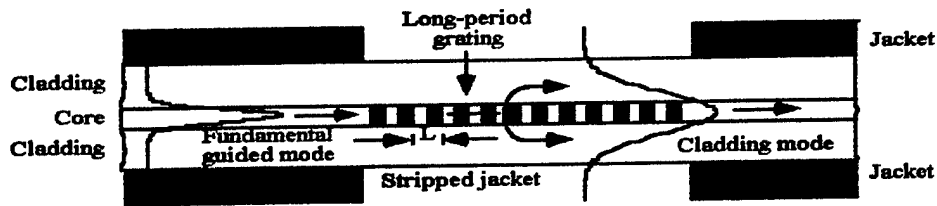
**Figure 3. Schematic of long-period grating sensor.**

Scientists at Lucent Technologies have demonstrated a type of photo induced grating in which the grating spacing is on the order of hundreds of microns [Vengsarkar, 1996]. Based on this grating periodicity, the phase matching condition is satisfied such that the forward propagating fundamental mode is coupled into propagating cladding modes and the electric field extends out of the optical fiber. As with fiber Bragg gratings (used for temperature and strain measurements), only certain wavelengths are affected. If the cladding is surrounded by air, then these cladding modes are guided by the glass-air interface, and they propagate with little attenuation. If, however, a lossy polymer jacket, such as those used on normal telecommunications fibers surrounds the cladding, then the cladding modes quickly attenuate and are extinguished by the interaction of the electromagnetic field of the cladding mode with the lossy jacket. Figure 4 shows a typical spectral response of an LPG filter. The absorption bands correspond to multiple cladding modes.
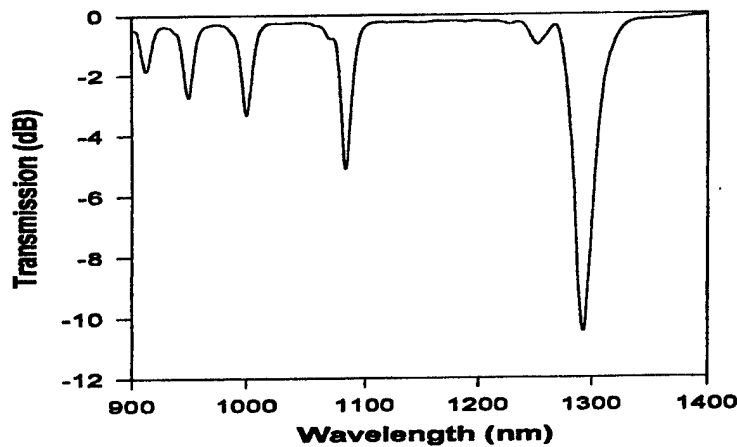
**Figure 4. Transmission spectrum of an LPG. The discrete, spiky loss bands correspond to the coupling of fundamental guided modes and discrete cladding modes.**

Thus, the LPG is a spectral loss element that scatters out light at a particular wavelength based on grating period, fiber refractive index, and the refractive index of the surrounding environment. This coupled wavelength can be designed for an isolated response to the refractive index of the surrounding environment.
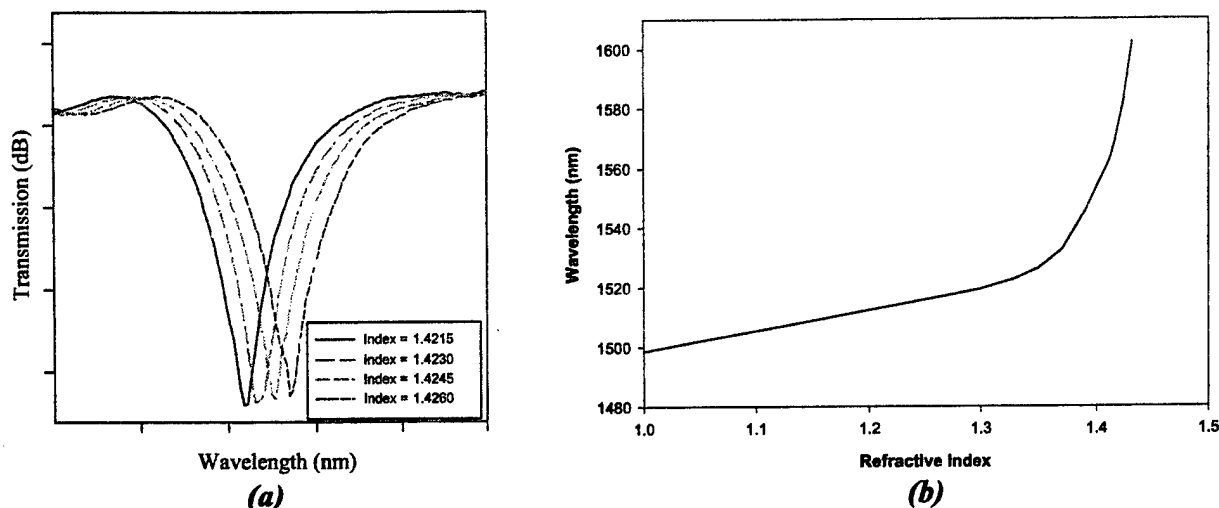


**Figure 5   a) Typical LPG transmission spectrums for different refractive index solutions.**
**b) LPG response to refractive index change is asymptotic.  Maximum refractive index resolution is seen in the higher (>1.35) refractive index range.**

Figure 5a shows a representative spectrum shift with refractive index change for a LPG sensing element.  The magnitude of this spectral shift can be tailored by adjusting LPG fabrication parameters.  Figure 5b shows the non-linear response of wavelength versus refractive index for this LPG sensor element.  By tracking the location of this spectral loss dip, real-time refractive index measurements can be accomplished.


## 4.    DETAILED DESCRIPTION OF RESEARCH PROGRESS

### 4.1    Optimize the pH sensitive hydrogel coating.

One of the objectives of the Phase II program was to develop pH sensitive hydrogels that would be used in combination with the enzyme organophosphate hydrolase (OPH), which catalyzes the hydrolysis of organophosphate containing compounds and produces a localized pH change. Several pH-sensitive polymer coatings were explored during this program including polyacrylamide (PAAm), poly(acrylic acid) (PAAc), poly(acrylamide-co-N-isopropyl-acrylamide) (PAAm-co-PiPAAM), poly(acrylic acid-co-N-isopropylacrylamide) (PAAc-co-PiPAAM), polyallylamine (PAAmine), poly(4-vinyl-pyridine) (PVP) and polyethylenimine.  The effects of monomer concentrations and polymerization procedures on the LPG pH sensors were investigated in commercial buffer solutions from pH 4.0 to 10.0.  All polymers were covalently bound to the LPG fiber surface through multi-step chemical reactions.  First, the LPG fibers were

extensively cleaned and dried then silanized with the appropriate chemical reagent to add the necessary functional groups onto the fiber surfaces. These functional groups were finally used to couple the polymer to the fiber through reagent-mediated procedures.

## 4.1.1    The "pH" LPG sensors based on polymer coatings from monomers.

Phase I results demonstrated that a very thin polymer layer coated on the LPG fiber was able to detect pH change based on pH-sensitive polymers. A pH sensitive fiber was prepared by layering, through ionic interactions, monolayers of pH responsive polymers. This process was done by alternatively dip-coating a LPG fiber with poly (allylamine hydrochloride) (PAH) and poly (acrylic acid) (PAA). After ten monolayers were coated, which is approximately 10 nm thick, the sensor was ready for use. Figure 6 shows the response of an LPG sensor to pH change in the phosphate buffer solution.
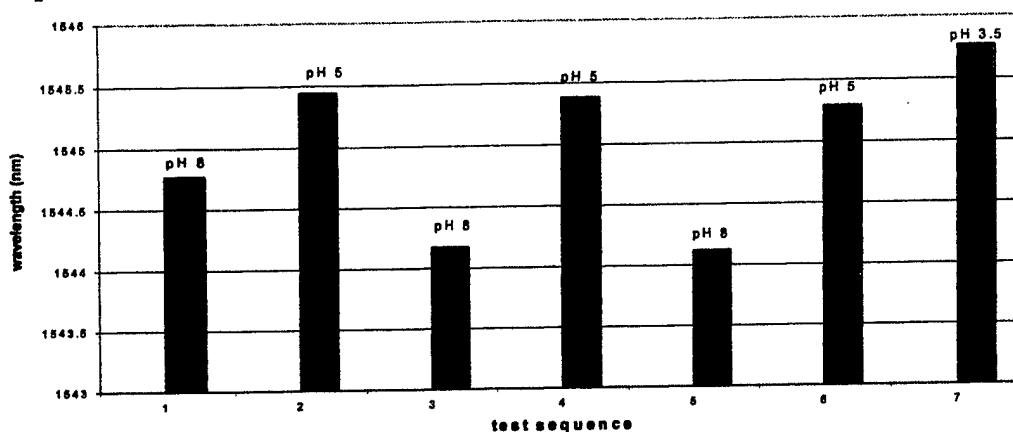


**Figure 6.  Sensor response to pH in phosphate buffer.**

An esterase was employed as a model enzyme for the Phase I program because esterase is the same type of enzyme as organophosphate hydrolase (OPH) and is readily available at a low cost. The esterase was immobilized in the monolayer structure through physical adsorption to the outermost layer. The immobilized enzyme was incubated with the substrate ethyl butyrate at concentrations of $10^{-4}$ M and $10^{-5}$ M. The response to the substrate is shown in Figure 7.
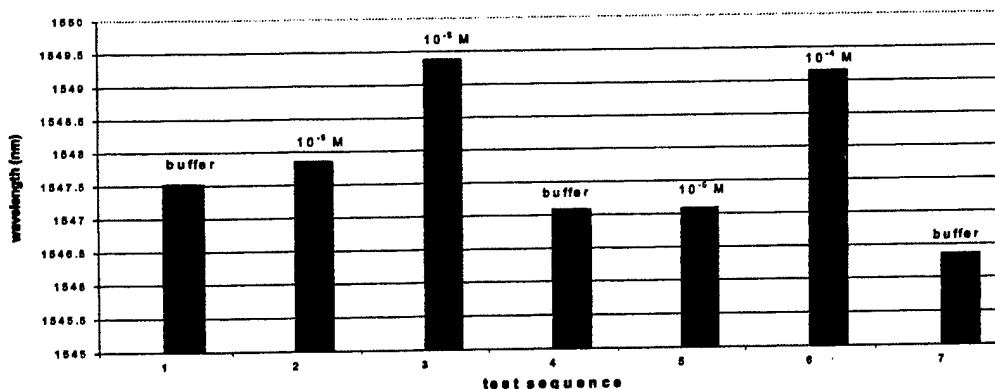


**Figure 7.  Sensor response to ethyl butyrate.**

14

Since polymer interaction through opposite charge is not very stable in aqueous media, a monolayer tends to dissociate gradually in a solution of high ionic strength. However, these results suggest that if a thin pH-sensitive coating is built through covalent binding, a stable sensor will result. Chitosans grafted with lactic acid have demonstrated novel pH-sensitive behavior in aqueous solution (Qu, *et al.*, 2000). The grafted chitosan forms hydrogels in aqueous solutions due to the physical crosslinking via hydrogen bonding and dipole-dipole interactions between neighboring ester groups and chitosan chains, as well as hydrophobic side chain aggregation. Luna employed chitosan oligosaccharide lactate (chitosan OL) as a pH-sensitive oligomer and covalently attached it to the amino-activated LPG fiber through 1-ethyl-3-(3-dimethylaminopropyl)-carbodiimide hydrochloride (EDC). The sensor demonstrated pH-sensitivity from pH 3.5 to 8. The graph in Figure 8 shows the test results.
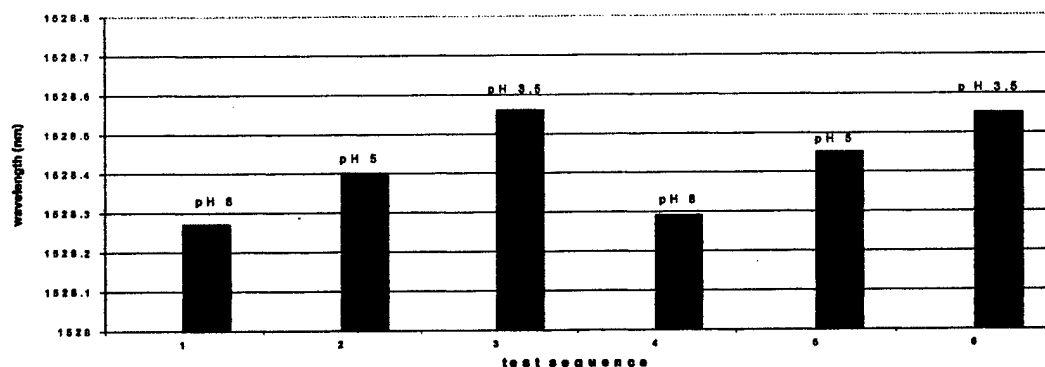


**Figure 8. Chitosan LA coated sensor response to pH.**

Esterase can also be covalently immobilized to the chitosan oligosaccharide lactate or amino-activated fiber through EDC activation to form amide bonds. By incorporating esterase in the process of attaching chitosan oligosaccharide lactate to the fiber, both chitosan and the enzymes are covalently bound either to the fiber or to the oligomer network. Covalent immobilization of enzymes also reduces the possibility of the enzyme leaching out of the polymer network, thus increasing enzymatic stability and lifetime.

Figure 9 illustrates the results of detecting ethyl butyrate with immobilized esterase in on the fiber. The sensitivity of the fiber is increased from $10^{-5}$ to $10^{-6}$ M of ethyl butyrate detection, which corresponded to a signal that was 10x over the noise floor of the system.
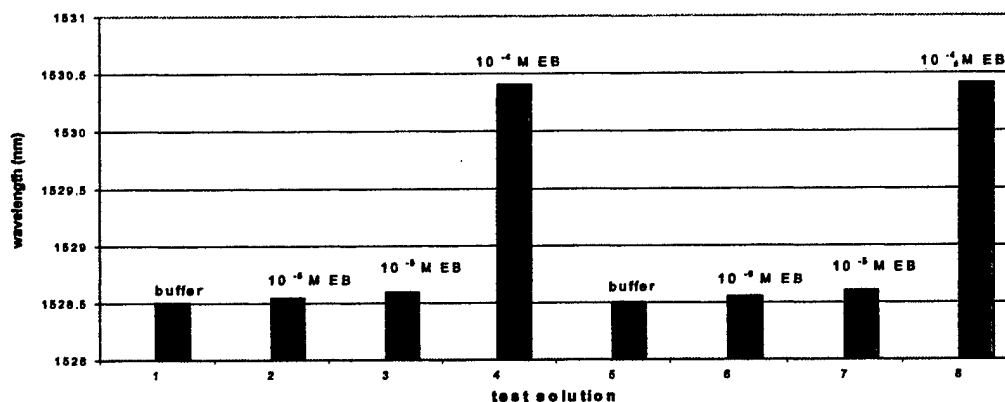


**Figure 9. Sensor's response to ethyl butyrate (esterase immobilized on Chitosan LA).**

A dose response to ethyl butyrate was performed and the following sensor-gram (Figure 10) was recorded. The y-axis corresponds to wavelength (nm) while the x-axis is time. The data demonstrated the dose response to ethyl butyrate in the concentration range of $10^{-6}$ M to $10^{-4}$ M.
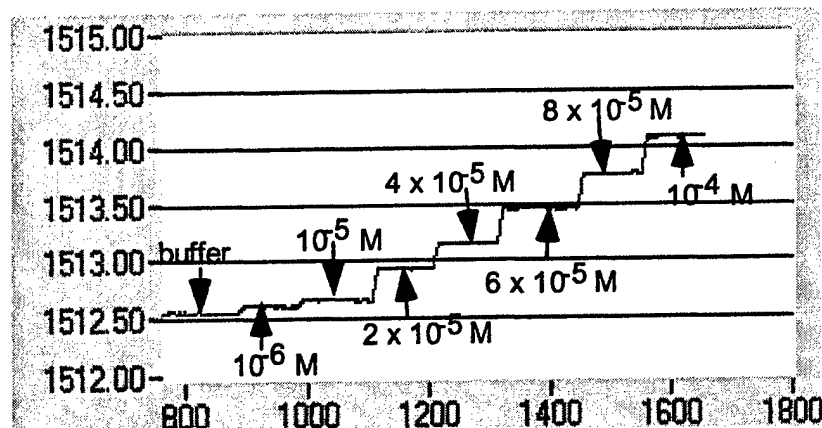


**Figure 10. Sensor-grams generated by the Lunascan demonstrating the dose response to ethyl butyrate.**

By plotting the wavelength number versus the concentration of ethyl butyrate a linear curve was generated. (Figure 11) Very good linearity was obtained in the concentration range from 0 to $10^{-4}$ M.
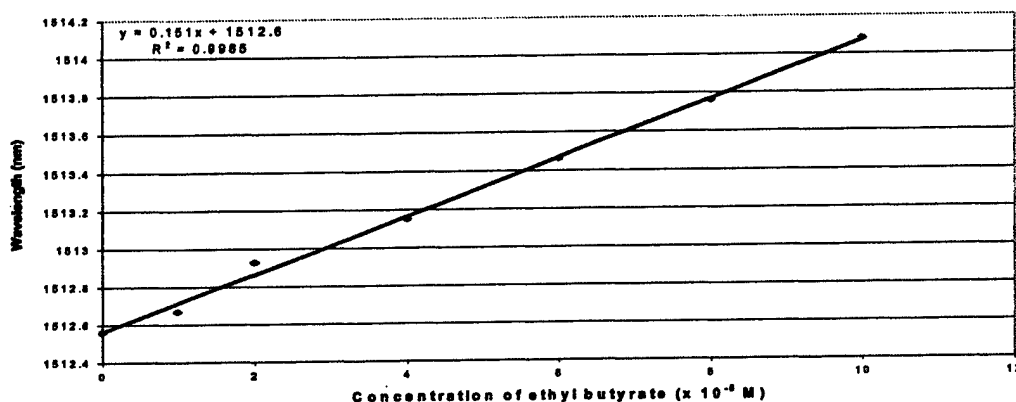


**Figure 11. Dose response to ethyl butyrate (esterase immobilized on Chitosan LA).**

**Construction of the "pH" LPG sensors based on polymer coatings from monomers.**
For the polyacrylamide, poly(acrylic acid), poly(acrylamide-co-N-isopropylacrylamide), poly(acrylic acid-co-N-isopropylacrylamide), polyallylamine, poly(4-vinylpyridine) coated LPG sensors, the procedures for covalent coating were as follows:

The surface of the fiber (LPG) was cleaned with 20% NaOH/ethanol (v/v = 1:1) for 2 hours and washed with de-ionized water. Then the LPG was treated with 2N HCl for 4 hours to introduce OH groups on the surface, washed with de-ionized water and ethanol, successively, and dried. The LPG was immersed in 10% [(3-(trimethoxysilyl)propyl methacrylate ethanol solution in

16

nitrogen environment for 6 hours to introduce carbon-carbon double bonds onto the surface, and washed with ethanol. The silanized LPG reacted with the solution containing monomers (acrylic acid, 4-vinylpridine, acrylamide, allylamine, and N-isopropylacrylamide), initiators (2,2'-azobisisobutyronitrile, 2,2'-azobis(2-amidinopropane) dihydrochloride, cross-linker (ethylene glycol dimethacrylate) by conducting UV irradiation for 15 min, and cured in an oven at 70 °C for 3 hours to enhance the polymerization. Prior to use, the LPG was immersed in de-ionized water for 18 hours to remove unreacted monomers and oligomers.

**Evaluation of the "pH" LPG sensors based on polymer coatings from monomers**
Single and multiple cycle pH profiling at room temperature was performed for every LPG. For every pH cycle profiling, 5 ml of buffer was filled in vials at a pH sequence of 4.0, 5.0, 7.0, 8.0, 9.0 and 10.0. Each LPG tested was equilibrated in de-ionized water for several minutes before proceeding with the experiment. After equilibration, the LPG was tested at each consecutive pH.

**Experimental Results based on polymer coatings from monomers**

*The PAAm-coated LPG sensor.*

PAAm is a nontoxic and water-soluble polymer. A PAAm polymer network can be easily formed by cross-linking monomers. The PAAm network is insoluble, but swellable in water. PAAm has widely been applied in HPLC and electrophoresis for separation of biomolecules. It is typically a neutral polymer sensitive to pH in solution. We coated PAAm on the LPG by polymerizing the monomer acrylamide on the surface of the LPG. To control the thickness of the polymer coating, the effect of the monomer concentration on the LPG sensor was investigated (Figure 12). The peak wavelength shift increased with the concentration of the monomer. The LPG sensor made from 1.0 M acrylamide and 0.005 M ethylene glycol dimethacrylate was used to explore the response to pH in buffers. The testing cycle was pH 4, pH 5, pH 7, and pH 10, which was repeated three times. The data is summarized in Table 1 and shown in Figures 13 and 14.

**Table 1. Summary of PAAm-coated LPG sensor response to pH.**

| Condition | N | Wavelength (nm) | SD |
|-----------|---|-----------------|-----|
| pH 4 | 3 | 1512.24 | 0.006 |
| pH 5 | 3 | 1512.22 | 0.017 |
| pH 7 | 3 | 1511.97 | 0.036 |
| pH 10 | 3 | 1511.86 | 0.025 |

The PAAm coated LPG sensor was most sensitive in the pH range of 5.0 to 7.0. The smallest peak wavelength shift was observed in the range of pH 4.0-5.0. The LPG sensor was least sensitive to pH from 7.0 to 10.0. To increase the amount of monomers, which react with the carbon-carbon double bonds on the LPG surface and form a thick layer of polymer on the LPG surface, the LPG optical fiber was immersed and polymerized in the monomer bulk solution without any crosslinker. The peak wavelength shift was increased from 0.40 nm to 0.55 nm, but it was hard to repeat these results. It is believed that the random radical polymerization initiated by UV radiation in the monomer bulk solution without crosslinkers could not be controlled effectively due to the variation of linear polymer chains.
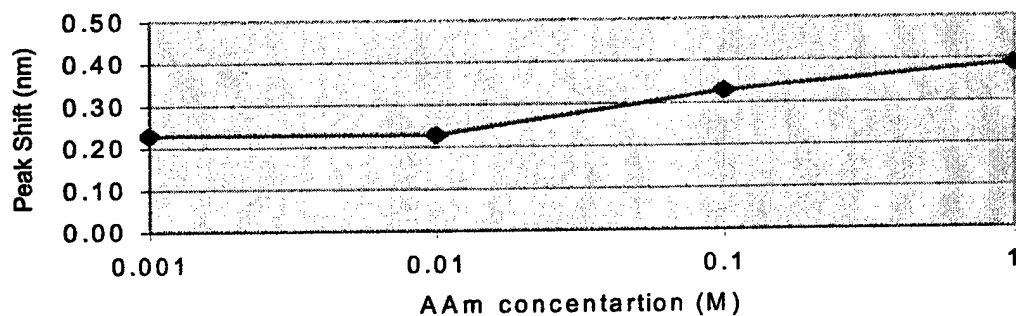
**Figure 12. Peak wavelength shift versus concentration of acrylamide.**
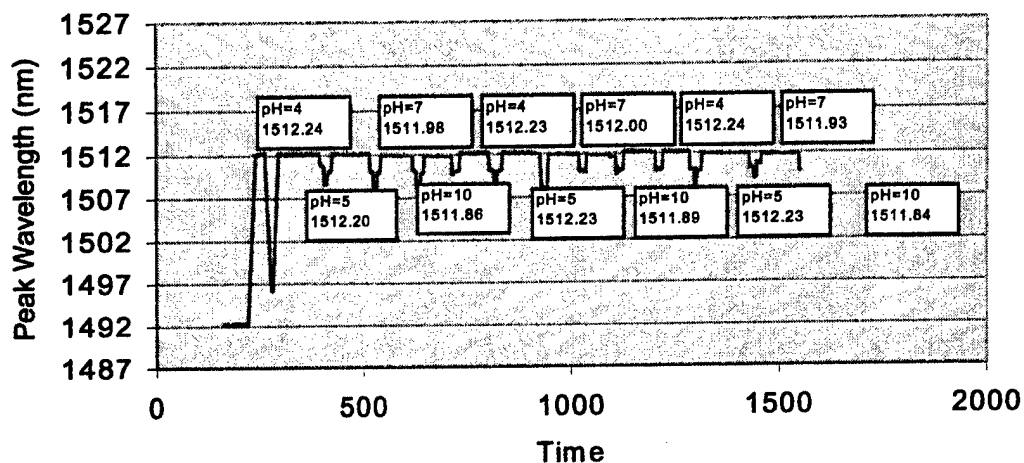


**Figure 13. Spectra showing multiple cycles of pH profiling of a PAAm coated LPG sensor responding to various buffers from 4.0 to 10.0 of pH.**
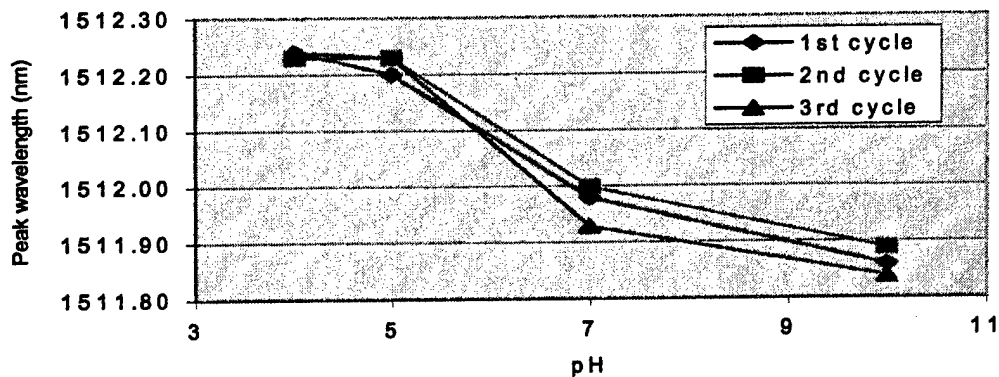


**Figure 14. pH of buffer solution versus peak wavelength of a PAAm coated LPG sensor.**

*The PAAc-coated LPG sensor.*

Poly(acrylic acid) (PAAc) is a water-soluble polymer that can easily be cross-linked. It is typically the carboxyl groups on the polymer chain that contribute to pH sensitivity in solution. We coated PAAc on the LPG by immersing and polymerizing in the monomer bulk solution without any crosslinker. The monomer used was acrylic acid. The LPG sensors were tested for responses to pH as described before. However, the results were not repeatable with even the same sensor. Subsequently a crosslinker was included in the polymerization reaction to add some rigidity to the polymer network. Figure 15 shows the results of a LPG sensor made from 1.0 M acrylic acid and 0.005 M ethylene glycol dimethacrylate, a crosslinker. The peak wavelength shift increased slowly from pH 4.0 to 7.0, then decreased sharply from pH 7.0 to 8.0. The response was attributed to the COOH groups on the polymer becoming deprotonated to form COO- groups as the pH increased, thus the polymer had increased solubility and flexibility in the buffer solutions.
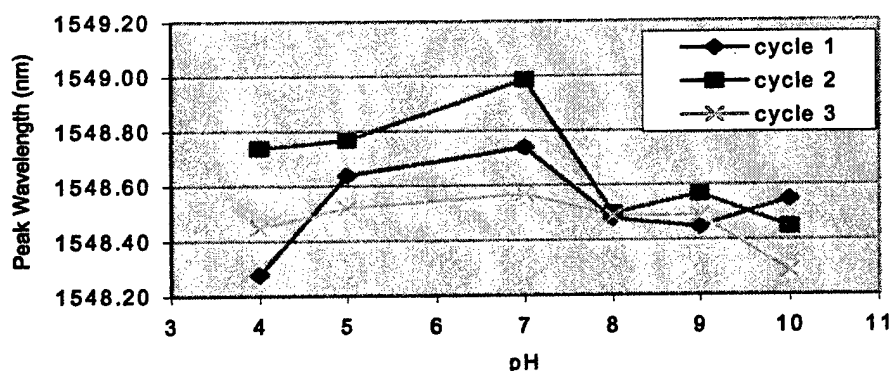


**Figure 15. Peak wavelength of a PAAc-coated fiber versus pH of buffer solution.**

*The copolymer-coated LPG sensors.*

In general, hydrophobic segments inserted in polymer chains increase swellability of the polymers. N-iso-propylacrylamide is more hydrophobic than acrylic acid and acrylamide. Poly(N-isopropylacrylamide) is water-soluble at room temperature, but insoluble above ~40°C. It has been used in controlled drug release such that solubility is dependent upon the environmental temperature. Luna tried a couple of copolymers with combined properties of polyacrylamide, polyacrylic acid and poly(N-isopropylacrylamide). The copolymers, poly(acrylamide-co-N-isopropylacrylamide) (PAAm-co-PiPAAM), and poly(acrylic acid-co-N-isopropylacrylamide) (PAAc-co-PiPAAM) were coated onto the LPG surface. Figure 16 shows the results of PAAm-co-PiPAAM-coated LPG sensor. The peak wavelength increased slightly from pH 4.0 to 5.0, then decreased from pH 5.0 to 9.0, with little change from pH 9.0 to 10.0. The trend of peak wavelength was repeatable, but the values were different for the same LPG sensor in different test cycles. The peak shift was much less when compared to the PAAm-coated LPG sensor, which contradicted the idea that the co-polymer should have increased swellability. It was believed that N-iso-propylacrylamide reduced the chain length or N-iso-propylacrylamide increased the cross linking sites. The PAAc-co-PiPAAM coated LPG sensor showed similar results to the PAAm-co-PiPAAM-coated LPG sensor (Figures 17 and 18).
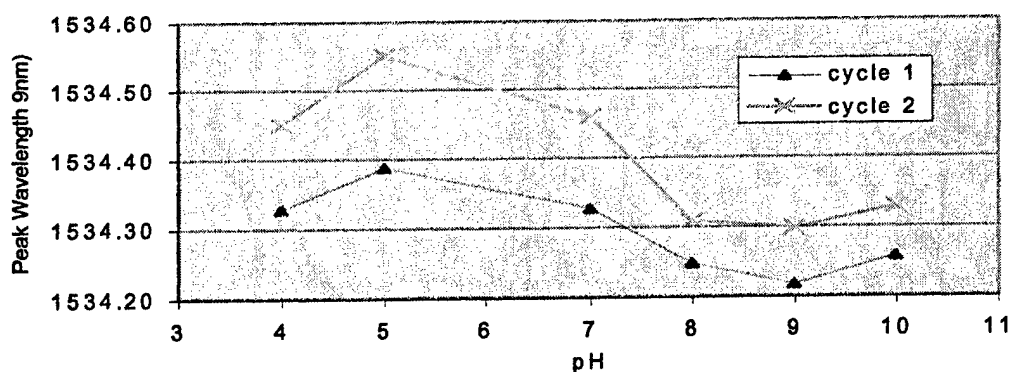
**Figure 16.** pH of buffer solution versus peak wavelength of a PAAm-co-PiPAAM coated sensor.



**Figure 17.** Spectra showing the multiple cycles of pH profiling of a PAAc-co-PiPAAM coated LPG sensor responding to various pH buffers from 4.0 to 10.0.



**Figure 18.** pH of buffer solutions versus peak wavelength of a PAAc-co-PiPAAM coated LPG sensor.

PAAmine and PVP are typical basic polymers sensitive to pH. In acidic solution, these polymers reacted with $H^+$ to form ammonium. Figure 19 shows the result of a PAAmine coated LPG sensor. The peak wavelength increased from pH 4.0 to 7.0, then decreased from pH 7.0 to 10.0. The peak wavelength shift was around 0.40 nm. The PVP-coated LPG sensor (Figure 20) was different from the PAAmine-coated LPG sensor. From pH 4.0 to 7.0, its wavelength decreased sharply, then slowly from pH 7.0 to 10.0. The sensor showed different sensitivity in different pH ranges, so the curve of pH versus wavelength was not linear. The peak wavelength shift was around 0.50 nm. The magnitude of peak wavelength shifts of both sensors was dependent upon the low molecular weight of the polymers.
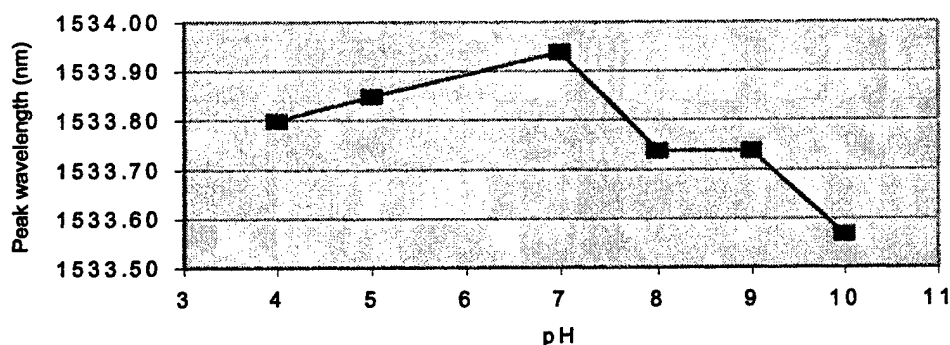


**Figure 19. pH of buffer solutions versus peak wavelength of a PAAmine coated LPG sensor.**
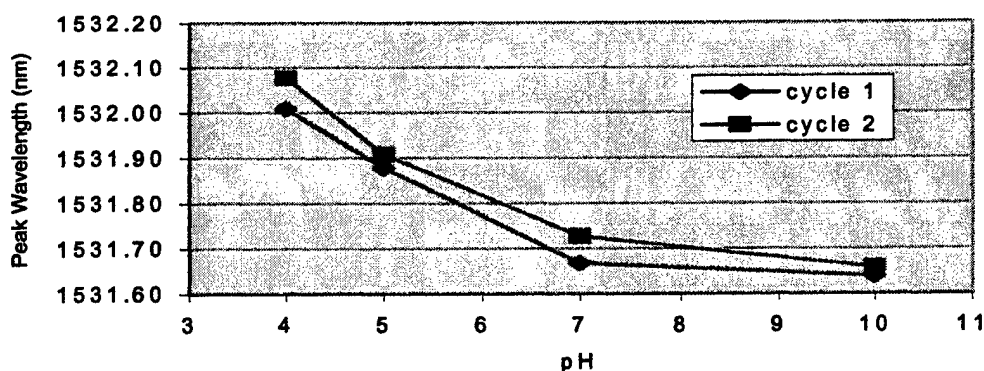


**Figure 20. pH of buffer solutions versus peak wavelength of a PVP-coated LPG sensor.**

### 4.1.2 The "pH" LPG sensor based on the PEI immobilization.

**Construction of the PEI immobilized LPG**

The surface of the fiber (LPG) was cleaned with 20% NaOH/ethanol (v/v = 1:1) for 2 h and washed with de-ionized water and then treated with 2N HCl for 4 h to introduce OH groups on the surface, washed with de-ionized water and ethanol, successively, and dried. The fiber was immersed in 10% 3-glycidoxypropyl trimethoxysilane (Aldrich, Milwaukee, WI) ethanol

solution in nitrogen environment for 6 h to introduce the epoxide groups onto the surface, then washed with ethanol. Finally, the silanized fiber was reacted with 2% polyethylenimine (Mw=750,000, Aldrich, Milwaukee, WI) for 18 h and then washed with de-ionized water.

### Evaluation of the PEI immobilized LPG sensor

Multiple pH cycle profiling for the PEI-immobilized LPG was performed at room temperature. For every pH profiling cycle, 5 ml of buffer was filled in vials at a pH sequence of 4.0, 5.0, 7.0, 8.0, 9.0 and 10.0. Each LPG tested was equilibrated in de-ionized water for several minutes before proceeding with the experiment. After equilibration, the LPG was tested at each consecutive pH after equilibrium.

### Experimental Results of the PEI immobilized LPG sensor

The pH cycle data is summarized in Table 2 and shown in Figures 21 and 22. The PEI immobilized LPG sensor was cycled five times from pH 4.0 to 10.0 at room temperature. The peak wavelengths of the sensor always decreased with increasing pH from 4.0 to 10.0 and showed the same trend during the 5 cycles. The difference of peak wavelengths between the maximum and minimum peak were around 1.5 nm

**Table 2. Summary of pH cycle with PEI coated sensor.**

| Condition | N | Mean Wavelength (nm) | SD |
|---|---|---|---|
| pH 4 | 5 | 1540.912 | 0.189 |
| pH 7 | 5 | 1540.40 | 0.34 |
| pH 10 | 5 | 1539.85 | 0.22 |
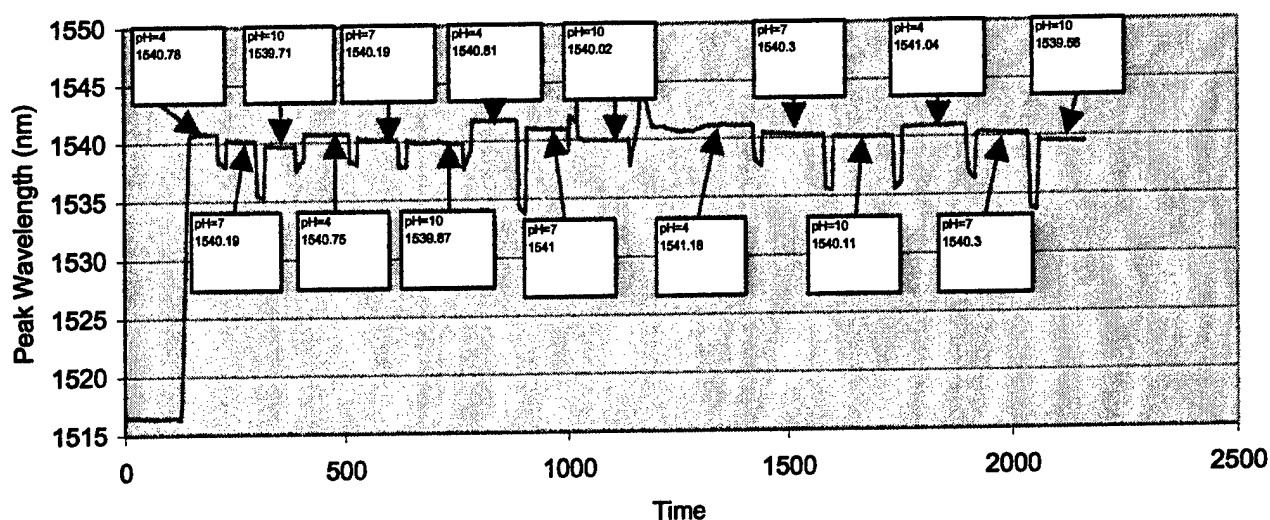


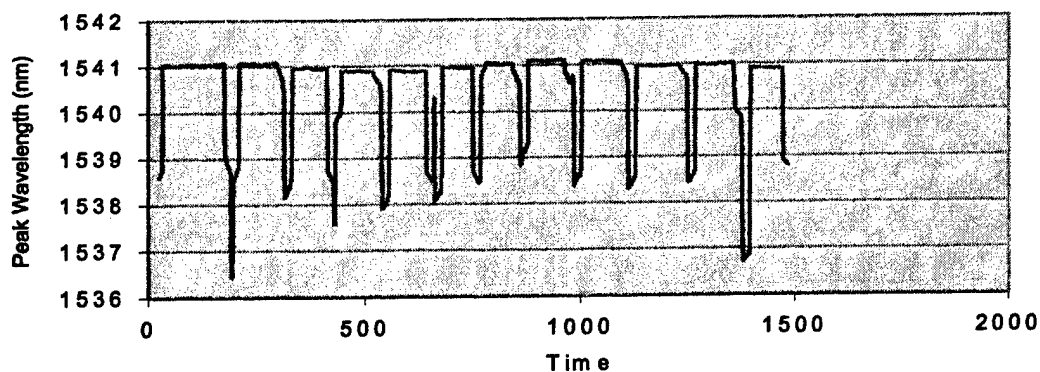**Figure 21. Spectra showing the multiple cycles of pH profiling of the PEI-immobilized LPG sensor I responding to various buffers from pH 4.0 to 10.0.**
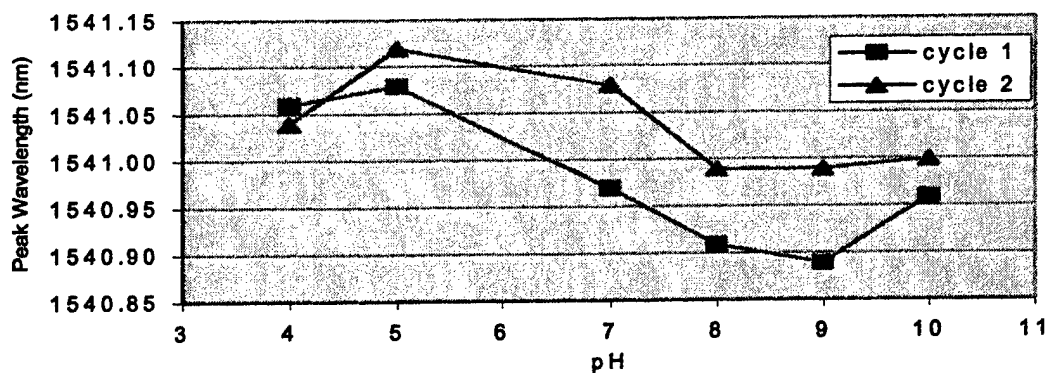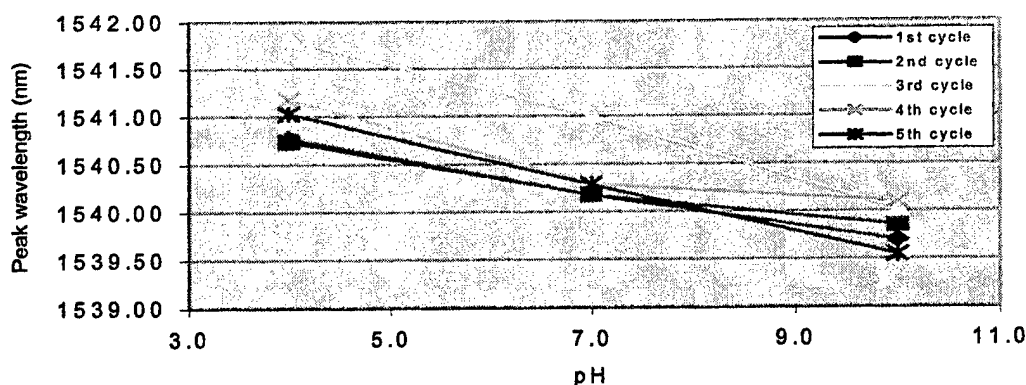
**Figure 22.  pH of buffer solution versus peak wavelength of the PEI immobilized LPG sensor I.**

Polymerization of polymer coatings on the surface of the sensor produced fibers that responded to pH changes with variability in wavelength shifts.  The amount of variability was the underlying issue to prompt the discontinuation of using pH swellable polymers with the organophosphate hydrolase and focus on the development of polymers that respond directly to the chemical warfare agents.  The development of direct response surface coatings is described in the following sections.

### 4.1.3  Development of reactive polymers for direct detection of chemical agents.

The following section describes the development of polymer coatings that were used to directly react with the mustard gas simulant tetrahydrothiophene (THT).

A nanomaterial and long-periodic grating (LPG) technology were used to develop the mustard gas sensor.  A mustard gas sensor was constructed by coating a composite of gold nanoparticles and PEI on the LPG fiber surface.  The sensor detected THT gas by monitoring the change of the refractive index of the interface of the LPG fiber in the THT gas surroundings.  When the THT gas reacted with gold nanoparticles on the LPG surface, the refractive index changed on the LPG fiber surface, which resulted in a wavelength shift.

Experimental Method.

*Materials:*  $AuCl_3$, 3-glycidoxypropyl trimethoxysilane, polyethylenimine (PEI, Mw=750,000) were from Sigma-Aldrich (St. Louis, MO).  NaOH, HCl and ethanol were from Fisher (Pittsburgh, PA).  Tetrahydrothiophene permeation tube was provided by KIN-TEK Laboratories, Inc. (La Marque, Texas).

*Construction of Long-Period Grating Mustard Gas Sensor:*  The LPG optical fiber was cleaned by immersing in 20% NaOH/ethanol (v/v = 1:1) for 2 hours, followed by rinsing thoroughly with de-ionized water.  Then the LPG fiber was treated with 2N HCl for 4 hours to introduce OH groups on the surface, washed with de-ionized water, ethanol and dried, successively.  After that, the LPG fiber was immersed in 10% 3-glycidoxypropyl trimethoxysilane ethanol solution in nitrogen environment for 6 hours, then washed with ethanol.  Next, the silanized LPG fiber reacted with 2% polyethylenimine for 18 hours and the sensor was washed with de-ionized water

to remove the adsorbed polymer on the surface of LPG fiber. The PEI immobilized LPG fiber reacted with $AuCl_3$ solution to form complexes of $Au^{3+}(NH-)$, which were used as crystal cores to grow the gold nanocrystals as show in Figure 23. Finally, the sensor was dried and ready for use.

Silanized LPG          PEI coated LPG          Gold nanoparticle
                                               immobilized LPG

Polymer          AuCl$_3$
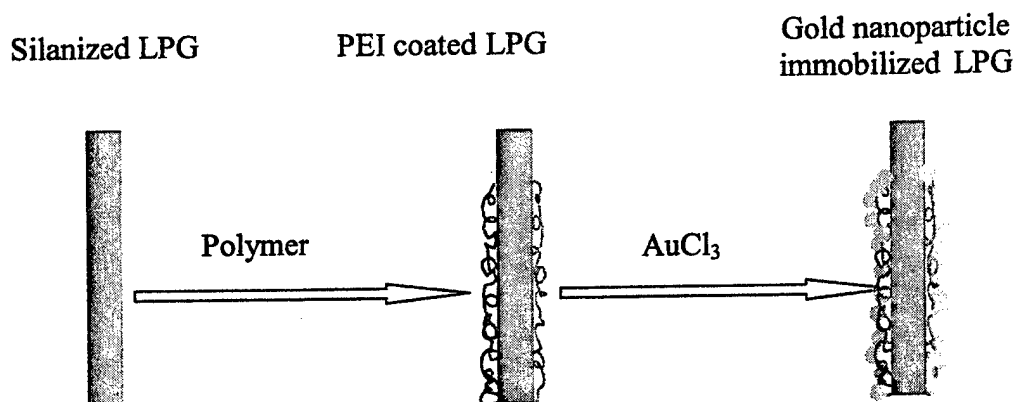
**Figure 23. Construction of LPG mustard gas sensor.**

***Generation of the tetrahydrothiophene (THT) sample:*** A THT permeation tube and a gas standard generator (KIN-TEK Laboratories, Inc. La Marque, Texas) were used to produce different concentrations of THT sample, a simulant for mustard gas, by adjusting $N_2$ flow. The permeation tube filled with THT has a permeable polymer membrane and is placed in a housing tube. When the THT permeation tube and housing tube are heated to 80°C, the THT vapor permeates through the polymer membrane and creates a small stable flow of THT. The small stable flow of THT is added to a much larger flow of carrier gas ($N_2$) to form a precisely controlled low concentration gas sample:

$C = f/F\ 10^6$, where C is the sample concentration, f is component emission at temperature T (1.086 ng/min at 80°C), F is dilution gas flow.

***Evaluation system of the sensor:*** The set-up of the evaluation system for the mustard gas sensor is illustrated in Figure 24. When the 50 cc/min $N_2$ is bubbled from tank 1 into the gas standard generator at 80°C containing a THT permeation tube (serial No. 29903), 5ppm THT is produced. Different concentrations of THT are obtained by mixing different flow rates of $N_2$ from tank 2 with the 5ppm THT produced from tank 1. Teflon tubing was used throughout the delivery system. The Luna Scan 3000 detected and collected the signals of wavelength shift. The computer recorded and analyzed the experimental data such as the output wavelengths. The mustard concentration can be correlated with the output wavelength shift from the LPG sensor.
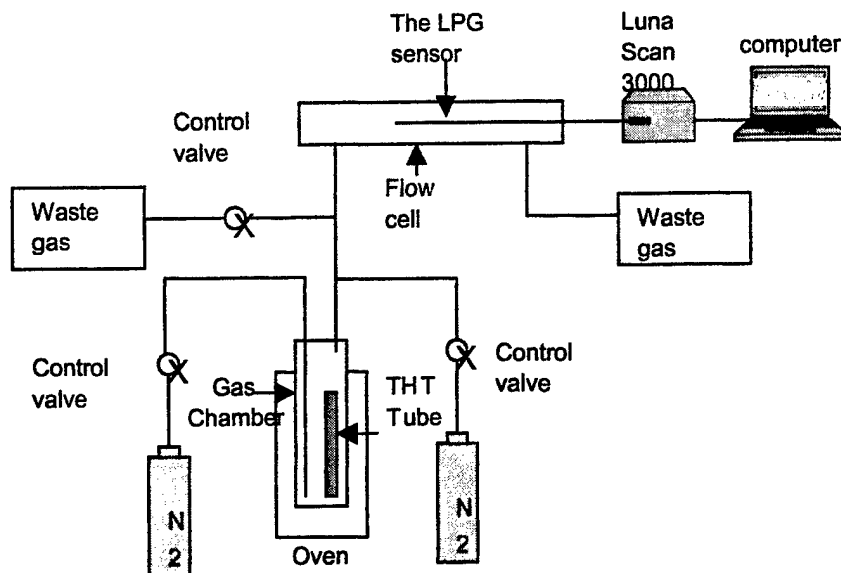
**Figure 24. Schematic of mustard gas sensing system.**

Figure 25 shows the typical sensor spectrum and the response of the sensor to THT. The peak wavelength increased slowly with time when the mustard gas flowed through the sensor in a gas flow cell. After an hour exposure, the wavelength shift reached a steady state. The slow change of wavelength shift could be explained as follows: it took some time to reach 1ppm THT after turning on the gas generator, (i.e., it took some time to reach the right temperature); while 1ppm THT-$N_2$ gas passed through the flow cell, the reaction of THT with the gold nanocrystals was a heterogeneous interface reaction, therefore, it took some time for THT to reach all surfaces of gold nanoparticles and react with Au. After all surface areas of the gold nanocrystals reacted with the THT molecules, no subsequent reaction occurred resulting in no further observed wavelength shift.

The effect of $AuCl_3$ concentration on the sensor was also investigated and the results are shown in Figure 26. When the $AuCl_3$ concentration was increased from 1 mM to 20 mM, the sensor wavelength shift increased from 0.07 nm to 0.41nm. This can be explained by the fact that more gold nanoparticles were formed on the LPG surface at higher $AuCl_3$ concentrations. This provides a larger surface area for THT to react and produces a larger wavelength shift. Due to the saturation of Au on the LPG surface, or larger nanocrystal surface areas at higher $AuCl_3$ concentrations, the output of wavelength shift did not increase further.
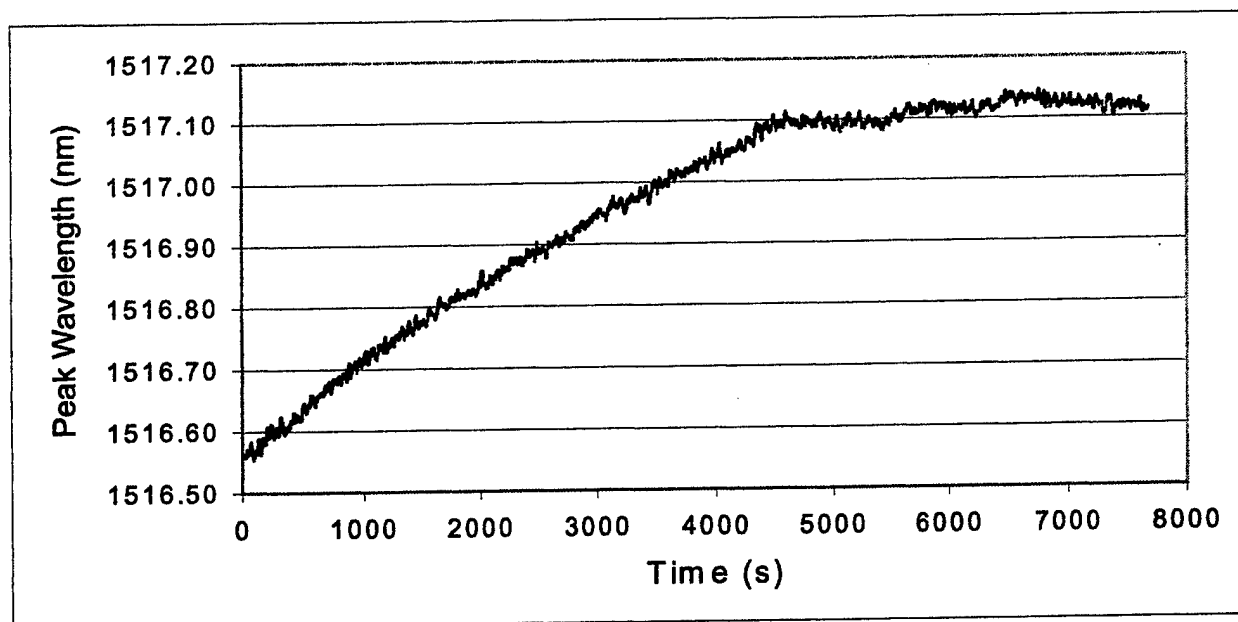
**Figure 25.  Typical spectrum of a THT sensor.**
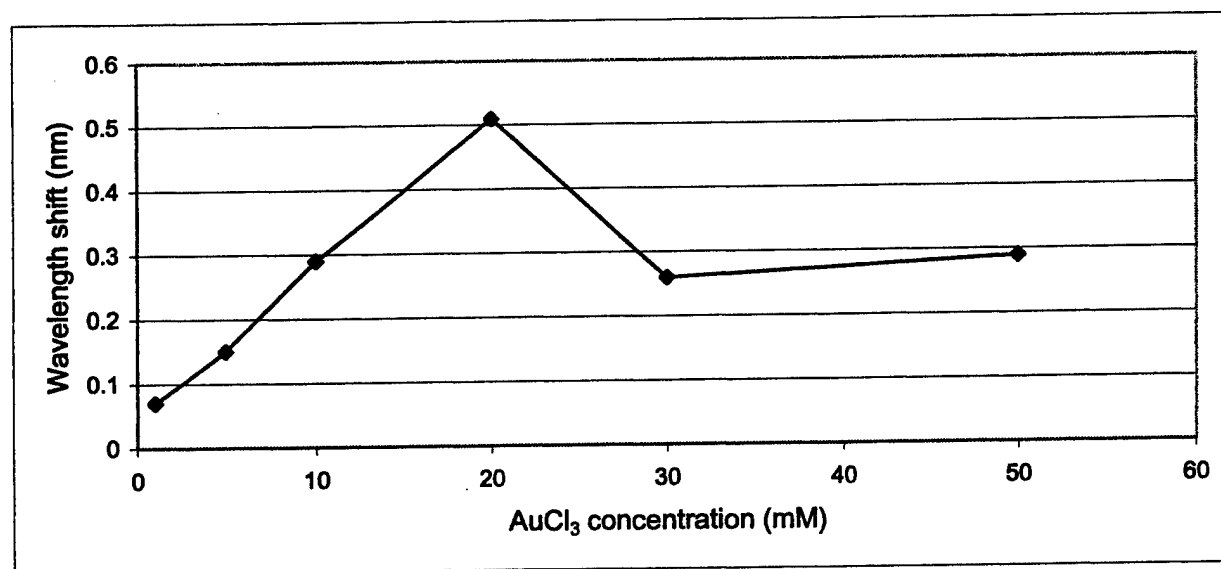


**Figure 26.  Wavelength shift versus AuCl₃ concentration used in the sensor construction.**

The PEI/gold nanoparticles coating on the LPG sensor provided a reactive surface for the detection of THT and subsequent detection by an observed wavelength shift in the spectrum of the LPG sensor.  This coating provided a means to further characterize the performance of the air sampling system during the integration with the sensor platform.

### 4.1.4 LPG sensor optimization.

As stated earlier, part of the Phase II development effort was to optimize the LPG in the 800 nm wavelength range. The components available for the signal conditioning within this wavelength range are four times cheaper, smaller, have a higher sensitivity, and are more robust. By transitioning the operating wavelength to 800 nm, there have been many enhancements made to the Lunascan 3000 LPG detection system. By optimizing the LPG operating in the 1500 nm range to work in the 800 nm range, Luna has been able to develop a more reliable sensitive system that is cheaper and flexible to the end user. These system improvements open various markets to Luna that were once restricted by price, size, and sensitivity with the 1500 nm system. Table 3 summarizes the differences between the original 1500 nm Lunascan system, and the current 800 nm Lunascan system. Performance of the system has been improved by over twenty-fold.

**Table 3. Summary of system changes made for optimization of the LPG platform.**

| Hardware | |
|---|---|
| Spectrometer | *Replaced $11,000 spectrometer with $600 component* – By changing the optical operating wavelength, a mechanical scanning element was replaced by a silicon CCD array, the same component used in digital cameras. |
| Signal to Noise | *Reduced noise by order-of-magnitude* – Noise floor levels were reduced from 0.02 nm to 0.002 nm, corresponding to an equivalent increase in sensitivity. Previous Lunascan averages data from over five seconds to achieve results. |
| Multiplexer | *Replaced multiplexer with more reliable system* – Vendor change resulted in a faster switching speed and an operating specification of greater than 100 million cycles. |
| Computer Interface | *Eliminated the need for data acquisition cards* – USB interface is now used creating a more reliable, standardized, data transfer package. |
| Internal Temperature Control | *Added thermal stabilizers to internal optics* – Temperature control of the optical source results in increased optical source lifetimes and lower noise levels. |
| Software Upgrades | *Developed windows-based software package* – User friendly software is compatible with hardware integration and data storage packages. |
| Sensors | |
| LPG-Design | *Developed reflection-based sensors instead of transmission* – Single-ended configuration enabled sampling flexibility and increased channel count. |
| LPG Design | *Improved sensitivity by 50 percent* – By changing the optical fiber and redesigning the LPG profile, greater responses to refractive index changes were achieved. |
| LPG Design | *Reduced the length of the sensing area* – Less intrusive sampling techniques needed and smaller sample volumes can be used. |
| LPG Manufacturing | *Improved manufacturing repeatability* – To support the increase use of sensors, the manufacturing process was changed to control sensor operating wavelength. |

The newly developed system consists of signal-conditioning electronics containing a source and spectrum analyzer, with a USB computer interface. Figure 27 is a photograph of the new Lunascan 3000 system that operates in the 800 nm wavelength range. In addition to increased sensitivity, cheaper components, additional features were added to the system for ease of use and flexibility through software and hardware. As shown below, in Figure 27, the front panel includes various operation lights that signal the user that the system is operating correctly. The fiber optic connector on this panel is a LC bulkhead that mates with the LC connector supplied with each sensor. This system can be operated alone with a single sensor or multiplexed with the optical switch shown in Figure 27c to monitor multiple channels.



(a)                                                                                          (b)



(c)
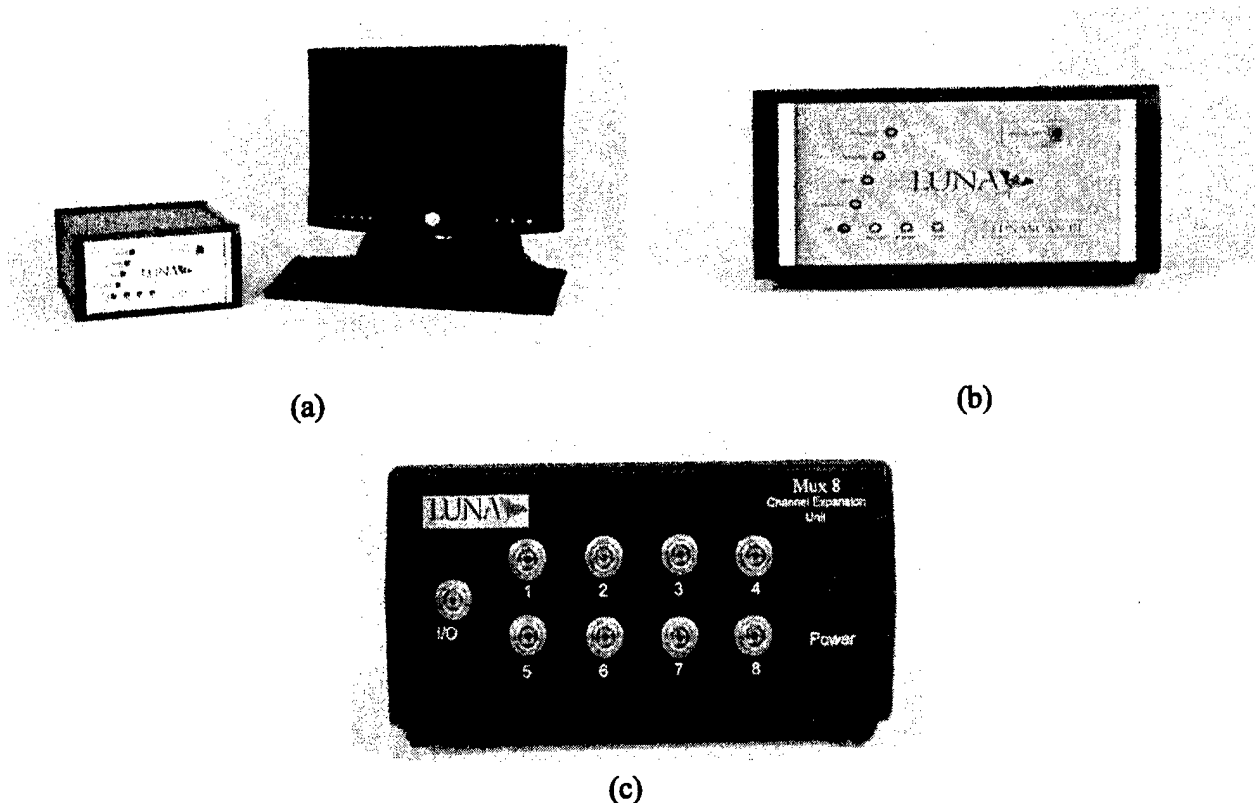
**Figure 27. Photograph of new Lunascan-3000 with USB computer interface operating in the 800 nm wavelength range.**

The newly developed Windows-based Lunascan software walks the user through system setup, system operation, data acquisition, data display and storage, and data analysis. The software addresses the Lunascan system through a USB connection to retrieve spectral intensity information, or the spectral content of the light received from each sensor. This data is obtained from a charged coupled device (CCD) array within the Lunascan-3000 system, a component similar to the detector used in digital cameras. The raw signal is then analyzed to determine the sensor operating wavelength, which correlates to refractive index or concentration seen by the LPG, or temperature seen by a Bragg grating or EFPI temperature sensor. This information is graphed versus time, providing a sensorgram on the PC screen. In addition, the data is stored to a file for later retrieval, additional analysis, and report writing. The user interface for the

Lunascan-3000 system is being designed with quick, readily accessible features. Multiple windows can be opened and customized, allowing the user to tailor his/her workspace for a specific application.

To support sensor operation, software was developed to interrogate the optical spectrum of the sensor strand and simultaneously track multiple spectral loss dips created by the LPGs. Also, the software allows the user to view the instantaneous spectral output from the LPG sensor. Using special algorithms, the user can track the spectral loss dip with time. This wavelength is correlated to refractive index and chemical concentrations. Figure 28, illustrates the new Lunascan software work space that can be tailored to the user. The software was used for development purposes only and will be leveraged into other development programs.
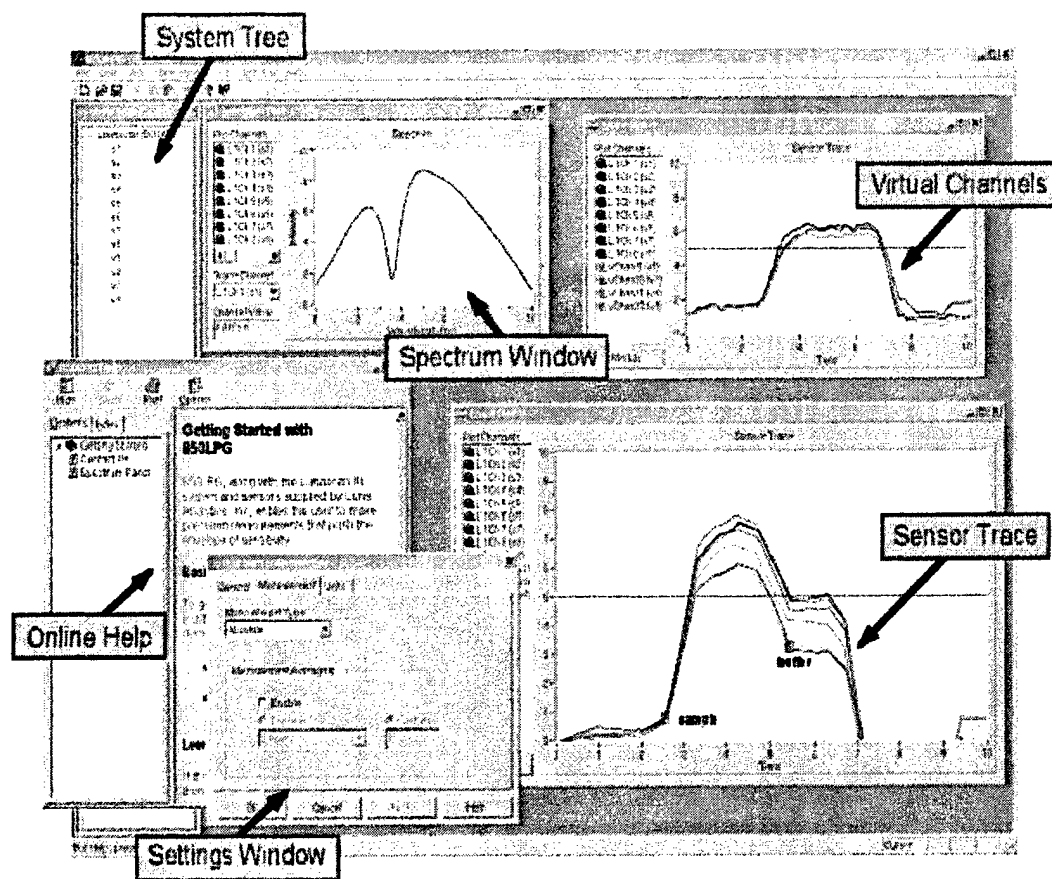


**Figure 28. Screen capture of the software graphical user interface illustrating configurability of workspace.**

The user can view multiple windows simultaneously with full operation functionality during testing. The application software will acquire and display data from multiple real and virtual channels for data analysis on the fly. System setup and online help windows can be accessed simultaneously if desired. Also, the user can access the **System Tree** window that is used for system setup and continuous monitoring of system operation (more than one Lunascan system can be run through this software).

Figure 28 shows all the critical windows that can be viewed through the software. For each sensor channel, there is an optical spectrum that is repeatedly acquired during testing. The Lunascan system continuously analyzes this spectrum to determine the wavelength or refractive index data displayed in the **Trace Plot** window. The **Spectrum Plot** is a useful tool to check the optical signal received from the fiber optic sensors. Each sensor cartridge will be delivered with a spectrum plot that can be downloaded and used to setup and calibrate before testing. It is good practice before operation, or during troubleshooting, to check the optical signal from the sensor channel ensuring proper sensor operation and connection. The **Spectrum Plot** window with a typical sensor response is illustrated in Figure 29 as well. The current sensor reading and a plot showing the optical power vs. wavelength relationship for each selected channel are displayed in this window.
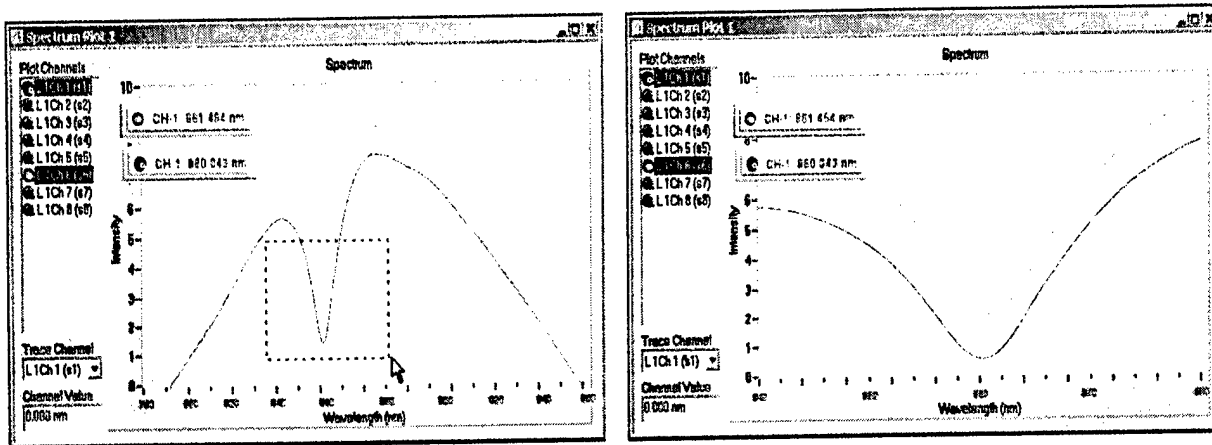


**Figure 29. Spectrum plot window displaying: optical response from Channels 1 & 6, zooming capabilities, and additional wavelength display windows.**

The **Spectrum Plot** window displays the spectra for each selected channel as it is acquired. Multiple spectra can be displayed on the same graph by selecting the sensor in the list to the left of the graph. The user has the capability of zooming and panning, as well as basic functions for graph manipulation within this window. Functions for graph manipulation and presentation are available from a "right-click" menu when the cursor is on the graph. When right clicking on sensors to the left of the graph, formatting options specific to each sensor are available, as well as the general sensor preferences.

The **Trace Plot** window displays the wavelength or refractive index versus time data for each sensor channel as well as virtual channels that are defined by the user. The sensors to be displayed on the graph can be selected from the list to the left of the plot. As shown in Figure 30, the user can add in markers to keep notes during operation. The interface for this window is much the same as with the Spectrum Plot. The user is capable of zooming and panning, as well as other basic functions for graph manipulation within this window. Functions for graph manipulation and presentation are available from a "right-click" menu when clicking on the graph. When right clicking on sensors to the left of the graph, formatting options specific to each sensor as well as the general sensor preferences are available. The user can turn on and off channel viewing at random, by clicking the channels to the left of the plot window.

30
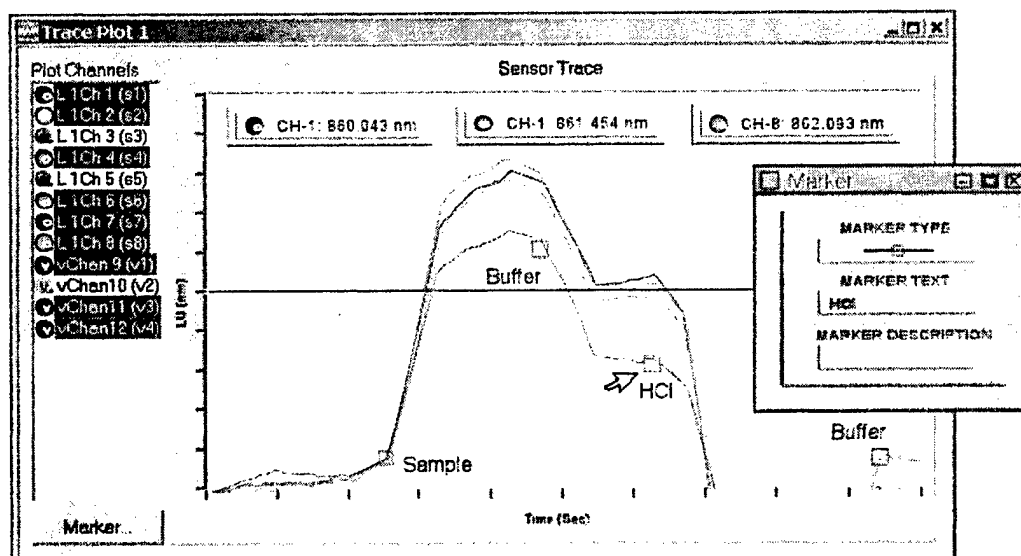
**Figure 30. Trace plot displaying kinetic binding data from sensor Channels 1, 2, 4, 6, 7, & 8, and virtual Channels 1 & 2.**

For future commercialized products, feedback from customers will be integrated into newer software versions with the ultimate goal of developing a multipurpose process monitoring tool.
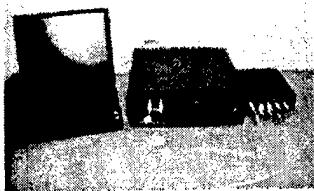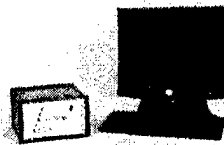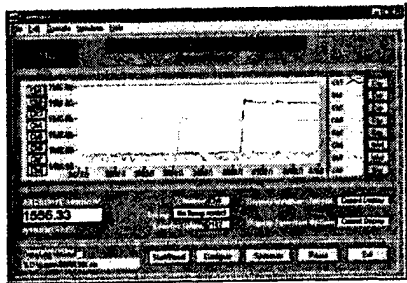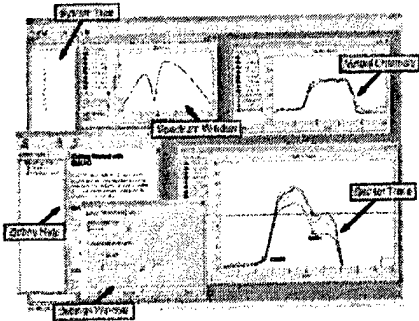
**4.2        Task 2. Miniaturize subcomponents.**

Specifically this development effort was focused on optimizing the refractive index sensor, and developing the air sampling system. The development efforts in Phase I showed that Long Period Grating (LPG) technology in the 1500 nm wavelength operating range was compatible for refractive index measurements. During Phase II, LPG refractive index measurement systems were developed in the 800 nm range. By transitioning the sensors from the 1500 nm operating range to the 800 nm operation range, sensitivity, cost, and flexibility were optimized to meet industry requirements. Table 4 illustrates performance upgrades made to the Lunascan LPG sensing platform.

**4.3        Task 3. Develop air-sampling system.**

Through continuous feedback and design reviews with Luna Innovations, Mesosystems has completed a MGS-sensor system design. Individual components of the complete system can be identified in Figure 31. These include the MGS shell and core, open/close window interface with solenoids, sampling fan and adapter, heat exchanger section, interface between fiber sensor housing and heat exchanger section, Luna's fiber sensor housing, interface between fiber sensor housing and downstream sampling pump, and a sampling micro pump.

31

**Table 4. Comparison of 800 nm and 1500 nm Lunascan detection System.**

| | First Prototype Lunascan system | Lunascan-3000 system |
|---|---|---|
| Operation Wavelength | 1500 nm | 800 nm |
| Sensitivity to RI changes | $2 \times 10^{-4}$ | $1 \times 10^{-6}$ |
| System Noise Floor | 0.04 nm (with temperature compensation) | 0.002 nm (with temperature compensation) |
| Speed | Scans every 10 sec | Scan every 7 msec – 1 sec data points |
| Computer Interface | NI DAQ acquisition cards | Easy to use, industry standard USB interface |
| Multiplexing capability | Works with a 1 x 8 channel switch | Software enables operation of up to 12 systems with an unlimited number of cascading optical switches. |
| Software capabilities | Standard software that acquires wavelength of LPG from 8 channels. Software logs and displays data. | New software that acquires LPGs from a number of channels. Allows the user to complete real-time post processing and temperature compensation with viewing capability. |
| Size (W x L x H) | 12" x 11" x 4" | 10" x 10" x 6" |
| Cost | $45K for single channel | $11K for system |
| Durability | System architecture includes mechanical parts that scan during operation. | System architecture includes <u>NO MOVING PARTS</u> |
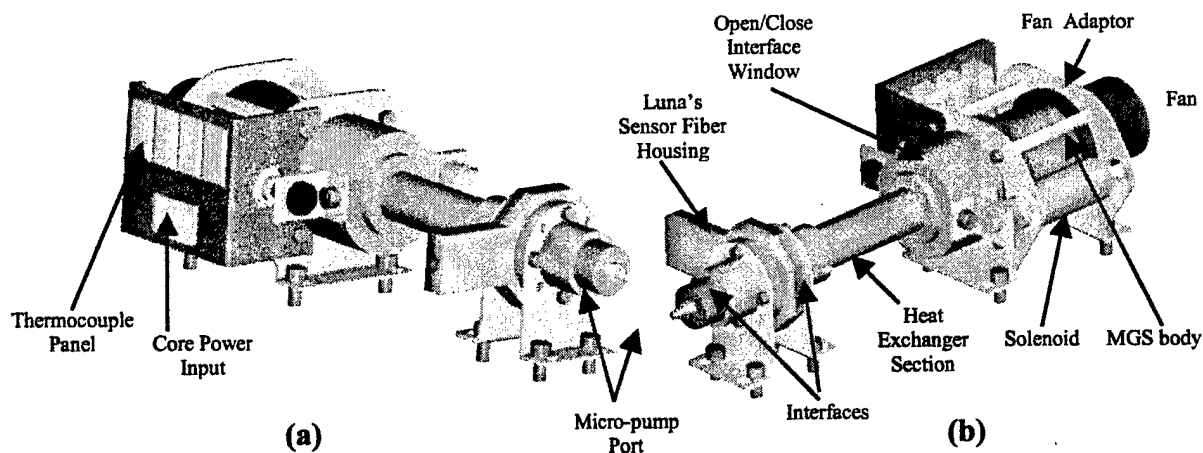
**Figure 31: ProE rendition of MGS-sensor system (a) left side and (b) right side.**

The process flow diagram of the integrated air sampling system and the long-period grating (LPG) sensor is shown in Figure 32. During the initial system initialization the temperature for the adsorbent core and heat exchanger regions are adjusted to the system set-points. The sampling fan is turned on (25 L/min) to draw external air across the Tenex core material. After 15 minutes of sampling the core temperature is ramped to 250 degrees centigrade to desorb the bound material. The desorbed sample is delivered to the LPG sensor, which is at 50 C, at a flow rate of 231 ml/min. Upon completion of the cycle, the initial sample core temperature set-point is established and the cycle is repeated.
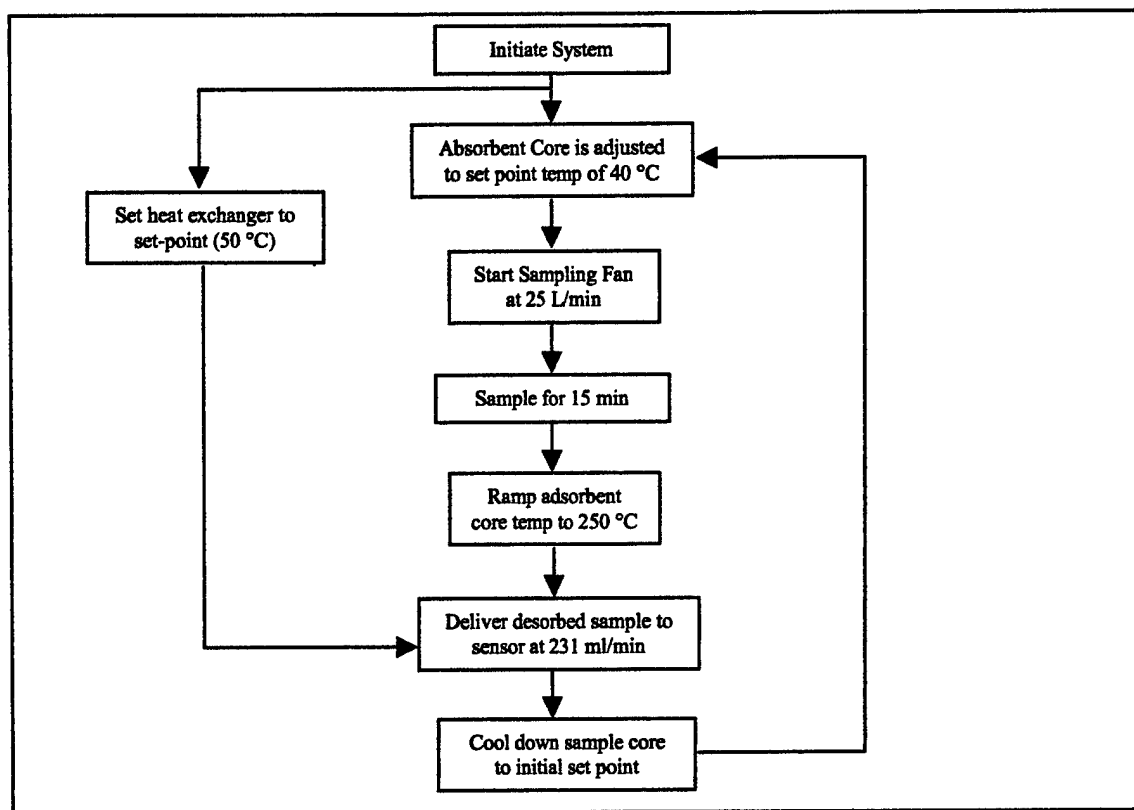


**Figure 32. Flow diagram of sampling process.**

Upon completion of the system design, Mesosystems has begun its focus minimizing weight and power requirements while maximizing concentration ability (i.e., optimization). Our main goal prior to this point was to design and fabricate a unit that performs well in lab and field demonstrations. A preliminary power consumption analysis was completed and conclusions drawn from the results act as our road map for moving forward.

Power Consumption Balance.

Important consideration has always been given to the power demands of the MGS device since the end product must be portable. During Phase I of this development, Luna engineers provided information relating to the available power. It was highly probably that the Douglas Guardian DG12-18, a 13.1 lb., 18Ah rated device would be the 12VDC source supplied. This acid battery can provide the following currents: 175A for 5 secs, 53A for 5 min, 11.5A for 1 hour. Assuming some regulation of this power is needed and minimization of the battery weight is necessary, Luna decided the best design target was 1.3Wh per sample cycle. In other words, given 12VDC the device demands 6.5A for 1 minute.

An analysis was completed to predict the total energy demand of the MGS-sensor system. Table 5 provides specific details relating to power requirements of the proposed system. This analysis assumes continuous monitoring with 4 minute cycle times. This generates a total of 15 cycles per hour.

**Table 5. Power requirements for each system component.**

| Equipment ID | Number of pieces | Operating time per cycle | Cycles per hour | Voltage supply (DC volts) | Amp Demand (Amps) | Power Demand Each (Watts) | Total Power Consumption (W-h) |
|---|---|---|---|---|---|---|---|
| Ledex 195202-29 solenoid | 2 | 25% duty for 0.5 sec | 15 | 12.1 | 2.31 | 28 | 0.12 |
| | | 100% duty for 10 sec | 15 | 12.1 | ·0.58 | 7 | 0.58 |
| Core Heater | 1 | 45 sec | 15 | 12 | 6.5 | 78 | 14.6 |
| Micronel Sampling Fan | 1 | Sampling for 30 sec | 15 | 24 | 0.055 | 1.32 | 0.16 |
| | | Cooling for 100 sec | 15 | 24 | 0.055 | 1.32 | 0.55 |
| 3VDC Sensidyne Micro Pump | 1 | Continuous | Continuous | 3 | 46.7mA | 0.14 | 0.14 |
| Resistance Heater (Watlow) | 3 | Continuous (?) | Continuous | 11.5 | 0.58 | 6.67 | 20.01 |

Clearly, the core heater and 3 heat exchanger resistance heaters create the largest power demand. Combined, these two components demand 34.6W-h while all other components cumulatively consume only 1.55W-h. Even if we assume only 2 cycles per hour, which reduces the core heater consumption to 1.95W-h, the power consumption is still dominated by the continuously operating resistance heaters (the heat exchange section).

There are several approaches to decreasing the power consumption of the heater core. As seen in Phase I work, providing an insulation layer between the heater core and the MGS shell will reduce heat loss. In this case, we have already implemented this strategy and little benefit will be seen by investing resources into new insulating materials. Another obvious approach would be to reduce the number of cycles per hour. This would prolong the life of the available power supply (battery).

Reducing the power demand of the heat exchanger section may be accomplished by decreasing the number of heaters, insulation of the outer surface, decreasing the flow rate through the heat exchanger, and/or decreasing the target temperature. There are pros and cons to each of these strategies, and these are discussed later in this report.

<u>Design and Test Heat Exchanger Section.</u>

Design and test a heat exchange section, which controls the gas temperature delivered to Luna's sensor fiber housing.

The completed gas concentrator-sensor prototype has several key demands that require a heat exchange section and have prompted the current heat exchanger design described here.

The first requirement is a controlled temperature environment for the sensor fibers. Luna Technologies provided a target temperature of 50 °C. This target value can change, but the key issue is to always provide the same temperature environment to the sensor fibers. This control ensures that calibrations made during manufacture hold true in a range of various operating conditions.

The second requirement is a minimization of CW agent adsorption on prototype surfaces. Most CW agents have a strong affinity to adsorb to cool surfaces (i.e., low volatility). Higher temperatures decrease undesirable adsorption and maximize material delivery to the sensor fibers. Our effort is focused on maintaining a constant outlet temperature (sensor delivery temperature) while maximizing the upstream temperatures.

The last requirement is a sub-category of the prior two. To maximize upstream temperatures while maintaining a constant controlled outlet temperature we must design an exchanger with excellent heat transfer characteristics. Metal monolith structures have good thermal conductivity between cells, high flowrate with low-pressure drop operation, and a large surface area for heat transfer.

## Heat Exchanger Fabrication.

Construction of the heat exchanger section was completed using a 700 cells per inch (CPI) spherical metal honeycomb monolith. The monolith honeycomb was approximately 0.59 inch OD and 3.75 inches in length. Watlow Kapton heaters were adhered to the outside surface of the monolith surface. A total of three heaters, each rated at 15W and 28V, were equally spaced down the length of the monolithic heat exchanger section. Each heater measured 0.87 inches in width and 3 inches in length. A total of four temperature monitoring locations were added to ensure a desired target of 50 °C was achieved downstream of the heated section (Figure 33).
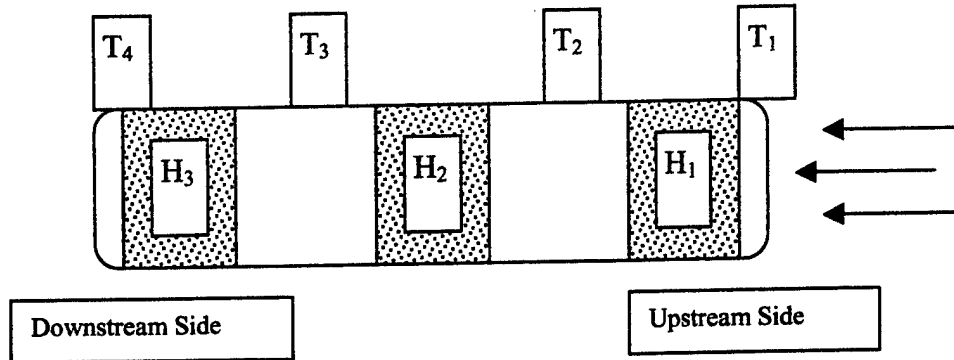


**Figure 33. Design concept of monolithic heat exchanger test device.**

Using a 0.047-inch drill bit, pilot holes to accommodated a 0.040-inch OD K-type thermocouple, were provided. Small gaps between the metal monolith and the stainless steel tube were filled with high-temperature silicone. Figure 34 illustrates the actual heat exchanger test piece used in the experiments that followed.
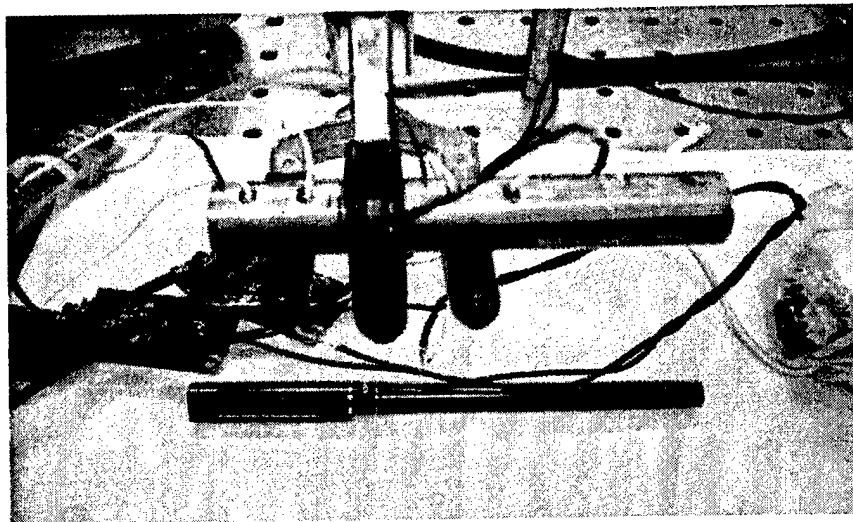


**Figure 34. Finished monolithic heat exchanger test device.**

36

## Experimental Setup for the Heat Exchanger Section.

Mesosystems' heat exchanger section was evaluated via the setup configuration observed in Figure 35. This experimental apparatus contained four elements: 1) an upstream gas pre-heater, 2) a monolithic heat exchanger, 3) a downstream sampling flow generated by a Sensidyne diaphragm pump, and 4) a 3-thermocouple temperature control system created at Mesosystems.
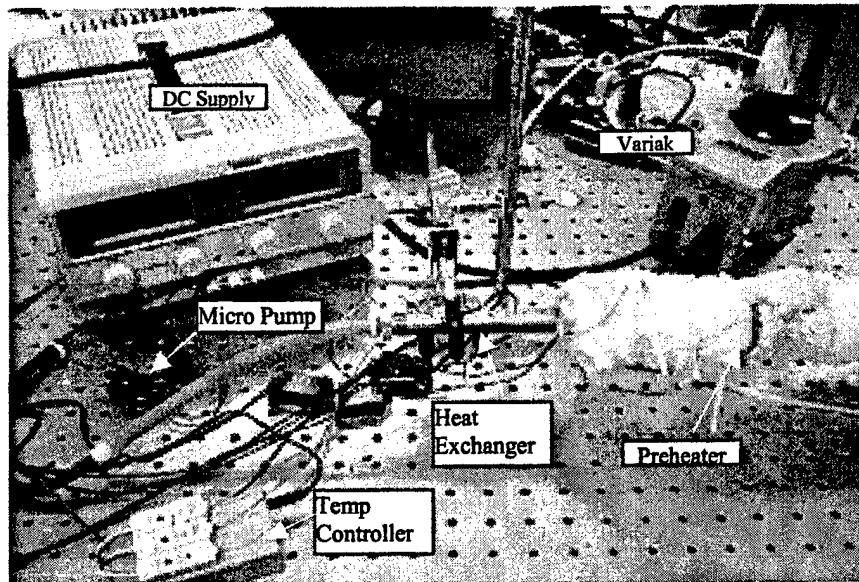


**Figure 35. Experimental setup for heat exchanger proof-of-concept and performance testing.**

The pre-heater section consisted of metal tubing, graduating up to meet the heat exchanger diameter, wrapped with resistance heaters. The temperature of the pre-heater section was manually controlled with a Variak to adjust power input to the resistance heaters. Temperature was monitored with a K-type thermocouple at the leading edge of the exchanger section. The result was hot gas (~250 °C) delivered to the entrance region of the monolithic heat exchanger section. The downstream sampling pump provided the suction power to draw the hot gas across the heat exchanger.

Sensidyne manufactures a large array of very small diaphragm pumps. Their smallest commercially available pump is rated for 3VAC and supplies a volumetric output of 231ml/min with no head pressure. This pump was used to draw a sample flowrate through the preheater and heat exchanger section.

A real-time temperature control system was created at Mesosystems to test our heat exchanger design. Our control system allowed for continuous monitoring of 3 thermocouple locations and feedback control of 3 resistance heaters. Again, a Variak was employed to provide power to the resistance heaters. The k-type thermocouples were positioned immediately after each resistance heater section. This design minimized any lag in temperature response and allowed for tight temperature control.

Experimental Results for the Heat Exchanger Section.

The heat exchange section was tested and the data was recorded into an Excel spreadsheet. The individual heaters (H1, H2, & H3) were controlled and set to 70 °C, 60°C, and 50 °C, respectively. Power was delivered to the heaters through a Variak, which is capable of supplying 120V and 20A. A 38V supply voltage was given and the maximum amperage draw (during ramp up) was 2.0A. The typical amp demand while maintaining a set point was 0.25A. The pre-heated gas temperature, measured at thermocouple 1, was at 271 °C. While this is the temperature of the gas as it is desorbed from the Tenex core, the use of the heat exchangers will provide a final temperature of 50 °C to the sensor region.

Excellent control and response was observed during testing. Figure 36 provides a visual temperature histogram over the course of the first experiment. Experiment one involved a one-minute exposure of the heat exchanger to a 271 °C gas flowing at a rate of 231 ml/min (i.e., Sensidyne pump rate).
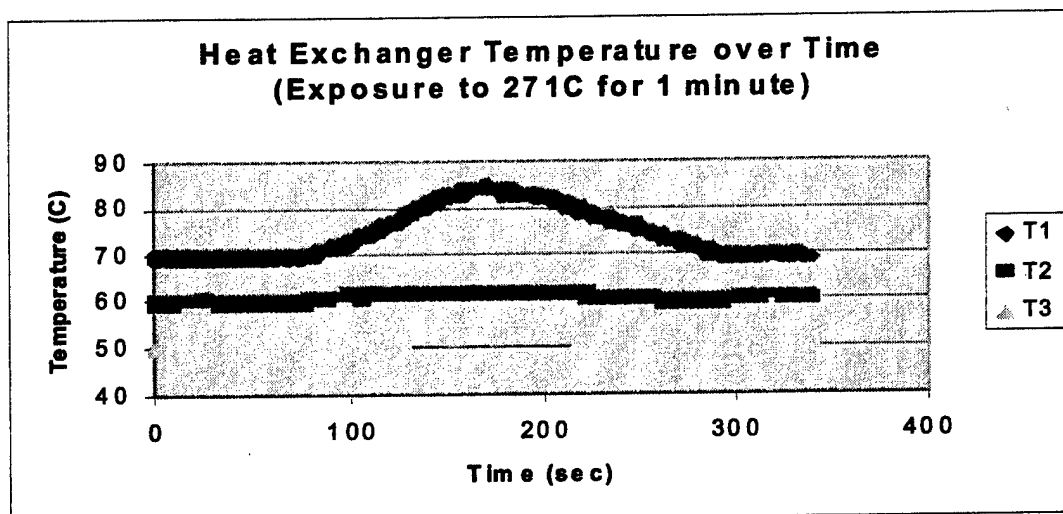


**Figure 36. Real-time heat exchanger temperature response (Exposure time = 1 minute).**

The one-minute exposure time is more than 6 times longer than a typical sample purge time and serves to ensure our heat exchanger is flexible in extreme operating conditions. Paying particular attention to thermocouple 3 (outlet point to sensor fibers) we observe a maximum temperature increase of 3 °C (50 °C to 53 °C). This temperature difference may exceed allowable temperature variance, but the exchanger performed very well given the duration of exposure and the temperature of the gas. In field operation, the maximum desorption temperature will likely not exceed 250 °C. Sample purge should not exceed 10 seconds.

An additional experiment was completed using a shorter exposure time of 30 seconds. The results, seen in Figure 37 below, provided evidence that the design would work. Following the temperature response of thermocouple 3 a maximum temperature increase of 1 °C was observed.
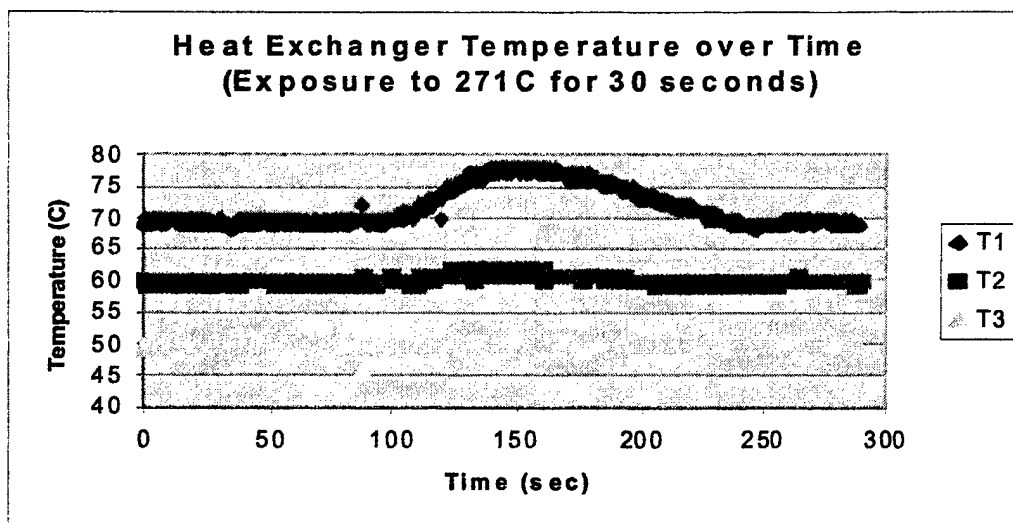
**Figure 37. Real-time heat exchanger temperature response (Exposure time = 30 seconds).**

Propane Testing.

Testing the performance of the gas sampler device with propane has been an experimental standard during most of the MGS development efforts. Propane is a high volatility, relatively safe, and readily available material that allows multiple, non-hazardous experiments, which aid in determining experimental protocol and relative performance. The experimental data obtained using propane is not representative of CW agent behavior, but serves as an experimental guide for more dangerous and difficult testing with materials such as chloroethyl-ethylsulfide (CEES), toluene, and dimethylmethylphosphate (DMMP).

Low concentration propane flows, metered by Mass Flow Controllers (MFCs), were created using a two-stage dilution. Starting with research grade propane, ~2 sccm 100% propane was combined with compressed-bottle air flowing at ~394 sccm. Approximately 16.7 sccm of this diluted flow was mixed with compressor air flowing at ~25 SLPM. The resulting mixture was ~3.1ppm propane delivered at 25 SLPM. The compressor air was stripped of water using a zeolite adsorbent prior to use. No treatment was given to the bottled air stream.

Through multiple trials, an experimental protocol was developed while using low concentrations (<10ppm) of propane as the analyte material. Sub-ppm level, 25 SLPM flowrates were delivered to the MGS device for a fixed sampling time (1-3 minutes). During sampling mode, the open/close-window-type interface remained open for low backpressure flow through the sampler. Once sampling was complete the open/close-window-type interface was closed manually. Power was provided to the heater and the temperature quickly rose (37 seconds) to 240 °C, at which time, the heater power was turned off. Within 4 seconds a purge flow was initiated, manually, to drive the sample to the FID.

A numerical value that quantifies the performance of the MGS is the "concentration factor." The concentration factor is defined as the analyte concentration in the MGS effluent (i.e., the concentrated sample) divided by the ambient or inlet concentration. Our results have shown that a reproducible concentration factor of 3 is achieved for propane when using the aforementioned

39

protocol and sampling a 3.1ppm-25SLPM flow, for 1 minute. A second test was performed by sampling for 3 minutes and we observed a reproducible concentration factor of 3.5. Table 6 provides summarized details of these two experiments.

**Table 6. Observed 12V-25LPM MGS concentration factor for propane at varying sampling times.**

| Initial Propane Concentration (ppm) | Max Ramp Temperature (°C) | Sampling Time (min) | Max Propane Signal Observed (ppm) | Concentration Factor ($ppm_{final}/ppm_{initial}$) |
|---|---|---|---|---|
| 3.1 | 240 | 1 | 9.8 | 3.2 |
| 3.1 | 240 | 1 | 9.2 | 3.0 |
| 3.1 | 240 | 3 | 10.6 | 3.4 |
| 3.1 | 240 | 3 | 10.9 | 3.5 |

It is important to mention that the results observed in Table 2 were obtained using a solid MGS cap with UHP $N_2$ being the purge gas. In a field environment, the sample purge strategy is to use the integrated high-volume sampling fan to direct the concentrated sample gas to a sensor. Clearly the most desirable situation would be to abolish the need for a secondary purge gas stream since portability is desired.

We believe that using a CPU fan to deliver a concentrated sample would cause little sample dilution. To test this assertion, two additional 3-minute sampling tests were completed using the sampling fan as the sample delivery hardware. Both experiments followed an identical protocol as mentioned previously except during the sample delivery step. In the first test, a heater ramp was initiated while the sampling fan remained in operation at 12V. In theory, functioning in this manner should result in a slight degree of dilution, but it simplifies the operation steps. In this mode, the fan serves as the sample collector and the sample delivery hardware while remaining "on" at all times. The second test followed a similar format, but the sampling fan was shut off after sampling and was not turned on until the desired desorption temperature (240°C) was reached.

In general, we observed the behavior predicted above. However, the resulting signal was much weaker than anticipated. In fact, the measured exit concentration was lower than the inlet feed concentration. Upon further investigation we discovered that our modified GC/FID configuration was responsible for the reduction in signal. The FID runs under a relatively small positive pressure, but this pressure was sufficient to exceed the ability of the fan to push the desorbed analyte toward the FID. Other analytical equipment devices, such as a MIRAN or SAWS detector, will likely have a vacuum-assisted or zero-pressure sample delivery, so use of the fan should be suitable in those applications and no purge gas is required.

## 2-Chloroethyl Ethyl Sulfide (CEES) Testing.

Previous testing during the 25LPM MGS development has been limited to propane and toluene. However, Luna innovations expressed interest in experiments using mustard gas simulants. Therefore, 2-chloroethyl ethyl sulfide (CEES) was selected as a representative material to predict the 12V-25LPM MGS device performance during mustard gas releases.

Low-ppm CEES sampling flows were generated using a saturator apparatus created in our laboratory. The saturator consisted of a carrier gas flow, delivered into a bed of small quartz beads, saturated with liquid CEES (98% Assay) purchased from the Sigma-Aldrich Company. The saturator exit stream CEES concentration was estimated based on the estimated CEES vapor pressure, the temperature, and the sweep-gas flowrate. Because a vapor pressure value for CEES was not readily available, we assumed diethyl 2,2-dichloride sulfide (commonly referred to as Distilled Mustard or HD/HS) was a representative material for predicting the vapor pressure of CEES. This value equals 0.11 mmHg at 25 °C.

The experimental procedure used in our recent propane experiments was also used during CEES testing. Concentration factor data for use of the MGS with CEES are shown in Table 7. As expected, a significantly higher concentration factor was obtained when feeding a 1.9-ppm CEES stream to the MGS at 25SLPM.

**Table 7. Observed MGS concentration factor for 2-Chloroethyl ethyl sulfide (CEES) at varying sampling times.**

| Testing Order | Initial CEES Concentration (ppm) | Max Ramp Temperature (°C) | Sampling Time (min) | Max CEES Signal Observed (ppm) | Concentration Factor (ppm$_{final}$/ppm$_{initial}$) |
|---|---|---|---|---|---|
| 1 | 1.9 | 240 | 1 | 50.9 | 26.8 |
| 2 | 1.9 | 240 | 1 | 63.3 | 33.3 |
| 3 | 1.9 | 240 | 1 | 58.7 | 30.9 |

All three concentration factors are approximately 30, but some of the variation is consistent with how the tests were run. For example, run 1 and 2 were run consecutively and it appears that an insufficient thermal treatment was provided. Run 3 data were collected after the MGS bed was thermally treated for 1 hour at 250 °C to ensure complete desorption of all adsorbed materials. The increase in peak concentration for run 2 (compared with run 1) is attributable to a small amount of CEES remaining in the MGS after run 1.

Considerations during 12V-25LPM field operations.

It is important to keep in mind that typical field operations will not see continued exposures to chemical agents without a thermal treatment protocol. A successful implementation of the 12V-25 LPM MGS is based on the assumption that once a CW agent is present, it is adsorbed (concentrated), desorbed, and detected by a sensor. Clearly, after an initial CW agent detection occurs, the MGS device must be regenerated to achieve the pre-existing baseline status.

In addition to CW agent exposures prompting an adsorbent regeneration strategy, the presence of significant levels of other organic materials in the environment will also force regeneration. During laboratory testing, no signs of background material accumulations were observed. However, this is likely to occur if the operating environment contains materials that strongly adsorbed, but are not of interest.

## Tenex-TA Degradation Investigation.

Concern over the stability of Tenex-TA in an oxygen environment, at elevated temperatures (50-400 °C), has become a key issue in the development of MesoSystems' gas sampling device. In previous testing and device development the availability of ultra high purity gas (i.e., UHP $N_2$ or He) was assumed and integrated into the sampling protocol. An experiment was conducted to determine if any degradation occurs when Tenax is exposed to oxygen at elevated temperatures.

A Tenex-TA adsorbent sample was evaluated via TGA/DTA/MS[1] during exposure to an inert gas (UHP helium) and to air as the temperature was ramped from 40 to 400 °C at 2 °C/min. A two-cup sample holder was employed, one with the sample and the other, the reference cup, containing approximately 440 mg of 30-50 mesh fused $Al_2O_3$, so as to allow for simultaneous DTA measurements. During the temperature ramp, simultaneous measurements were taken of sample weight, DTA signal and mass spectrometric data for mass numbers from 2-78. The adsorbent proved to be unresponsive in the inert environment. The MS data for all mass numbers was invariant throughout the run, as was the mass and DTA signal. However, in the presence of air, there was evidence of hydrocarbon combustion at temperatures above 300 °C, as evidenced by a sudden mass loss and the appearance of both water and $CO_2$ in the off gas. It is likely that CO was also present above 300 °C but it was not possible to distinguish between it and the $N_2$ in the sweep gas.

Figure 38 shows the result for heating in air. The onset of oxidation is approximately 300°C, as seen by the start of weight loss and the increasing $H_2O$ and $CO_2$ signals. CO was not detectible, since it has the same mass as $N_2$. The spent sample had changed from white to beige, also indicating that oxidation had taken place.
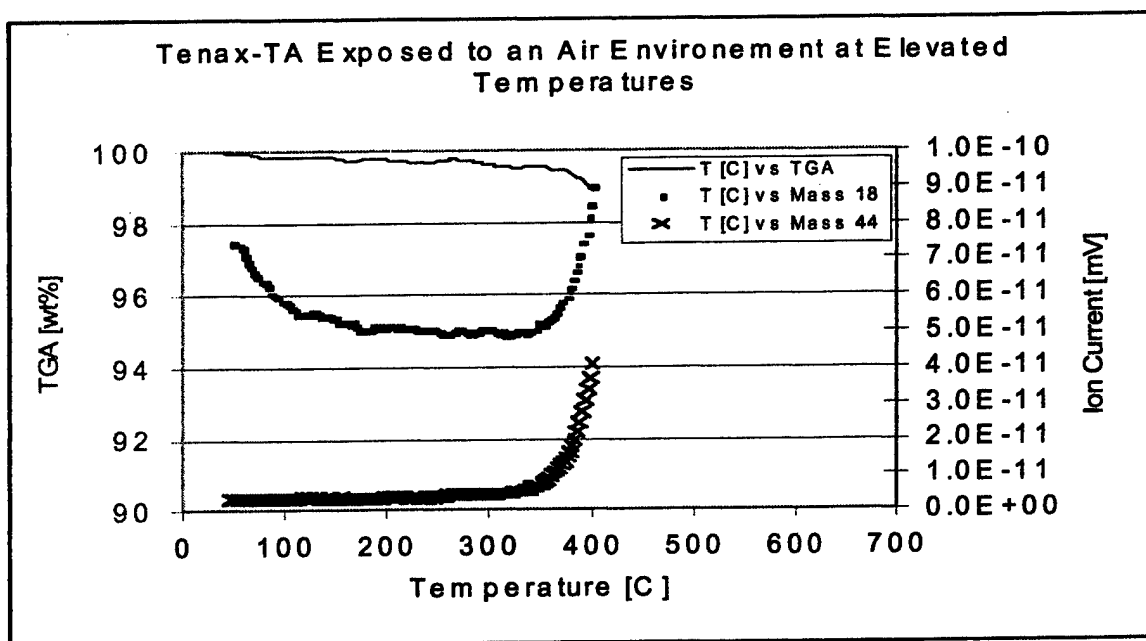


**Figure 38. Thermal behavior of Tenex-TA in air.**

---

[1] TGA – Thermogravimetric analysis; DTA – Differential Thermal Analysis; MS – Mass Spectroscopy.

Figure 39 compares DTA and TGA behavior in helium versus air. The mass change in helium is almost zero, which is consistent with the spent sample appearing identical to the fresh sample. DTA shows no events for either sample. The DTA peaks and mass changes below 100 °C are artifacts of the instrument behavior.
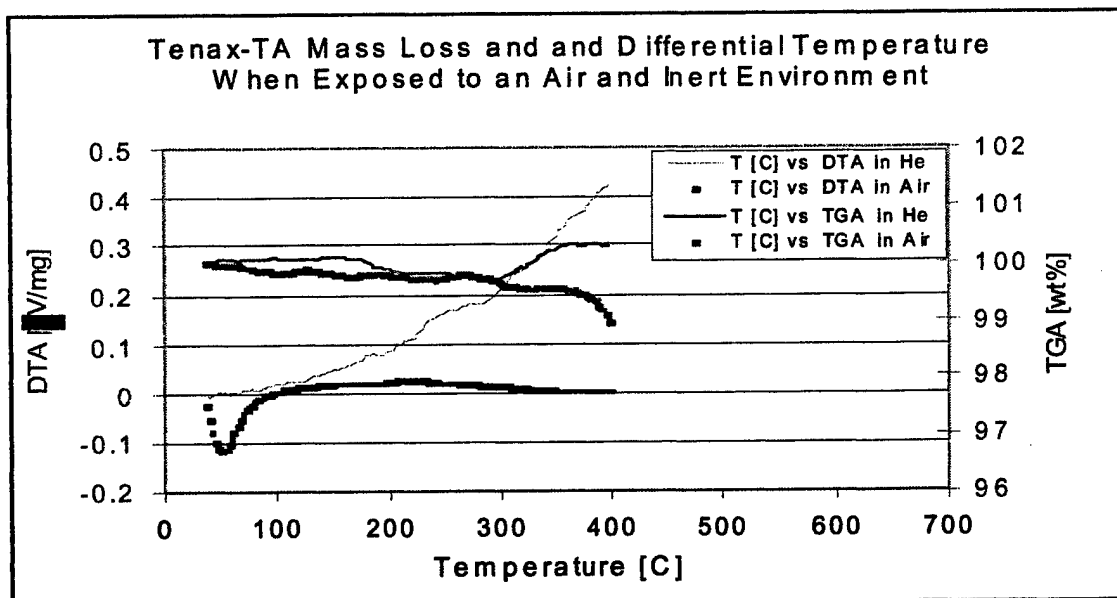


**Figure 39. Thermal behavior of Tenex-TA in air vs. helium.**

**4.4** **Task 4. Integrate subcomponents.**

The objective of the Phase II program was to produce a portable chemical detection platform with GPS and wireless networking capability. The LPG based sensor was also integrated with a MesoSystem air-sampling unit that would collect and concentrate the chemical vapor sample. To achieve this, the following subcomponents were integrated into the final chemical sensor system and are shown in Figure 40.

- Luna Aeroscan Digital Signal Processor Circuit Board
- Mini-Spectrometer
- GPS Receiver
- Wireless Transceiver
- Laptop Computer w/wireless interface
- Multiple SLED Light Source Circuit Board
- Sampler Controller Circuit Board
- Sampling Unit
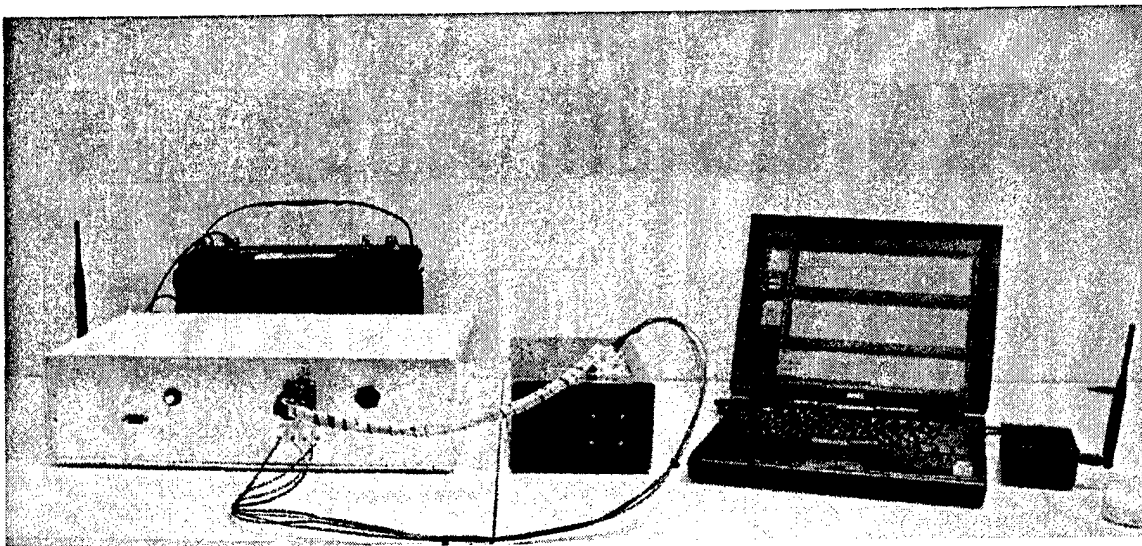- Power Regulator
- Battery

43

**Figure 40. Integrated chemical detection system.**

A system software package controls the integrated subcomponents of the chemical detection system. The details of the software are described in the following paragraphs.

Chemical Detection System User Software.

The Chemical Detection System is a master-slave type system. The master, or host unit, is a PC running Luna's AeroScan-PC Version 2.0 software, while the slave is the DSP-based data acquisition system in the remote sampling unit.

*Master Unit*

The PC software is designed to enable the user to configure the hardware data acquisition system, and view the data acquired from the sensors. The host connects to the remote system via an RS-232 connection, which can be substituted with a wireless cable replacement medium. Once connected, the software provides two data sampling modes: host controlled mode and standalone mode.

*Host-controlled Mode*

In the host-controlled mode, the system continuously scans each enabled sensor channel, and sends the processed data back to the PC immediately. This data then is plotted on a display graph, and can be logged to a data file.

*Standalone Mode*

With the standalone operation mode, the software tells the remote system to enter into a scanning loop where it takes data readings at a given time interval, defined by the user. Each data reading is stored in the remote system's RAM along with GPS position and time data. The GPS data is taken at the time of the sensor measurement. The PC software keeps track of the amount of data recorded, in terms of the amount of memory

44

available on the remote system. To gain access to the data logged in standalone mode, the user must first put the system back into host-controlled mode, so the system will be able to accept control messages from the PC software. The host can then request the remote system to send all data logged in memory, which in turn will be plotted on the display graph for analysis.

The PC software also includes diagnostic capabilities for viewing the spectrum output for each sensor channel. This is useful for sensor testing and development. Another function of the PC software is to enable user configuration of the remote system. This includes sensor channel configuration and calibration, algorithm configuration, and general system configuration parameters. Once all parameters are set, a flash programming utility will download all configuration parameters to the remote unit's nonvolatile flash memory, where it will remain until updated with a new configuration. Similarly, there is a flash programming utility available in the PC software to download new versions of firmware to the remote system, as they are released.

*Slave Unit*

The slave unit is a DSP-based motherboard, which controls peripherals used to acquire data from the fiber-optic LPG sensors. The DSP firmware operates as a slave device, meaning that it will not perform any operation unless told to do so from the Master unit, which in this case is the PC-controlled user software. The slave peripherals required for sensor data acquisition consist of an air sampler, laser light source driver, and spectrometer. The DSP uses various algorithms to drive these subsystems and process the sensor spectrum data returned from the spectrometer. The processed sensor data is then either sent up to the Master unit, or stored in the on-board memory, depending on the current acquisition mode.

Two additional peripheral subsystems include a GPS transceiver, and a 2.4 GHz radio transceiver. The DSP uses the GPS system to acquire GPS location and time information. This data is then associated with corresponding sensor readings. The radio system is used as the communications link to the Master unit. It is a pure RS-232 cable replacement system. The radio can be by-passed with the use of a special serial cable connecting the Master unit.

**4.5        Task 5. Test integrated system with simulants and interferents.**

The integrated system was evaluated with the mustard stimulant tetrahydrothiophene (THT) using a PEI gold-nanoparticle coated sensor. The THT was delivered from a permeation tube at a concentration of 10 ppm using nitrogen as the carrier gas. The carrier gas was sampled by the air sampler at a rate of 25 liters per minute for 4 minutes. The THT was adsorbed onto the Tenex core during this time period. The desorption phase was initiated following the 4 minute exposure phase by ramping the temperature of the Tenex core region to 250 degrees Celcius to desorb the THT. The desorbed material is delivered to the sensor region at a rate of 230 ml per minute for a 4-minute period. During the desorption phase the sensor is continuously monitored to detect any chemical agent in the desorbed sample. Figure 41 is a graph showing the response of the PEI gold nanoparticle sensor to 10 ppm THT. The control sensor is a non-coated LPG sensor and was run simultaneously with the test sensor. There is no response observed

with sensor two in the first test and very little response observed during second test. From the earlier testing with the PEI gold coated sensor it was observed that the maximum response time for this sensor was 60 minutes. The observed response of the sensor below can be explained by the limited exposure time of four minutes to the desorbed THT. The current configuration of the system would require a sensor coating that would respond to a desorbed sample in 10 – 30 seconds.
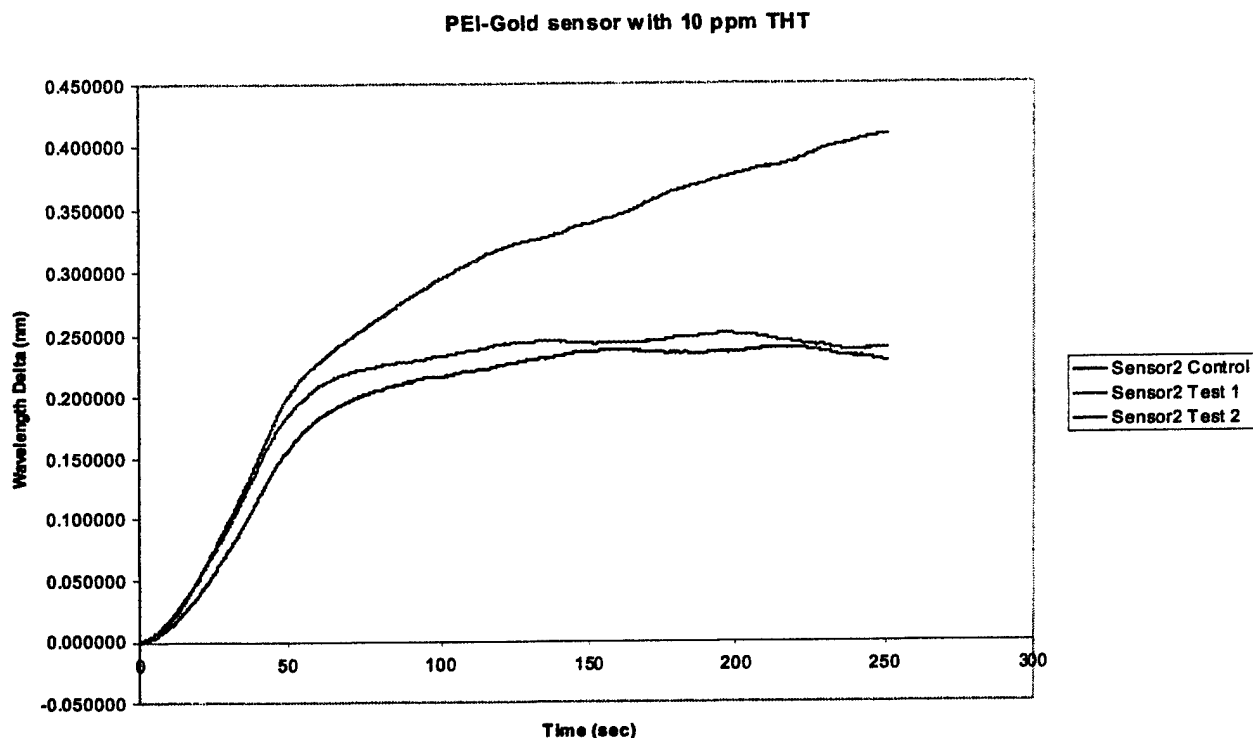
**PEI-Gold sensor with 10 ppm THT**



**Figure 41. THT testing with integrated system.**

## 4.6        Task 6. Establish commercialization plan.

The portable chemical detection system, under development during the Phase II program, has capabilities that span several commercial market sectors. Through a joint development and commercialization strategy, Luna Innovations has identified condition-based maintenance and oil exploration as two areas that will benefit significantly from the chemical detection platform. Toward this end, Luna has already sold multiple flight-qualified systems to Boeing and Lockheed Martin for use as aircraft dosimeters. The devices, which measure moisture, relative humidity and strain, have generated sales and purchase orders totaling over $150k. Additionally, work on the LPG platform has led in part to a relationship with Baker Hughes, Inc. Baker is interested in using the chemical detection platform for oil exploration, and as described in their support letter, has committed well beyond $250k to continue technology development.

Figure 42a illustrates the funds that have been obtained for further technology enhancements and resulting sales. Figure 42b is a photograph of the flight-qualified dosimeter.
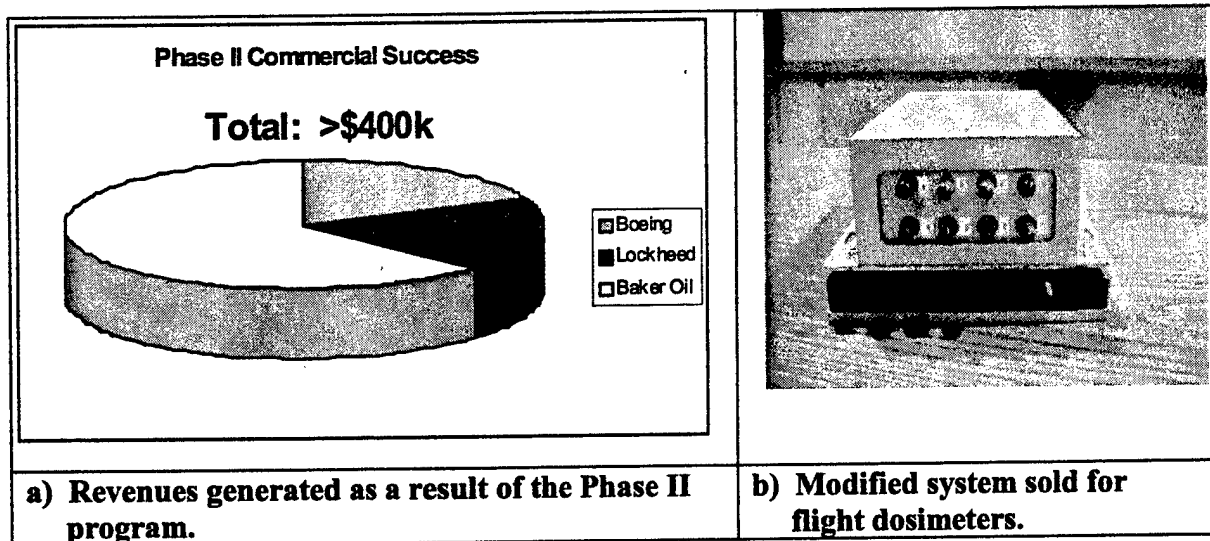
46

| a) Revenues generated as a result of the Phase II program. | b) Modified system sold for flight dosimeters. |

**Figure 42. Commercialization of Technology.**

Adapting the technology to down-hole environments presents many of the same challenges that now confront the defense community. The sensing instrumentation needs to provide effective, accurate performance, operate with minimal power consumption, detect chemicals in complex environments, and integrate with data fusion tools. Successful development of such a device will lead to tremendous cost savings and better exploration efficiency.

## 5.        CONCLUSIONS

During the Phase II program an integrated chemical detection was developed. The system consists of an air-sampling system for the collection of chemical vapor, an LPG sensor, wireless and GPS capability, and is also battery powered. The system was evaluated using the chemical simulant tetrahydrothiophene (THT), which is a simulant for mustard gas. The final testing produced inconclusive results during the detection process. Although the testing did not provide the expected results, the system hardware provides a tool to further evaluate coatings on the LPG sensor, which could provide viable detection capabilities. Further coating alternatives could be selected from polymers that are currently being used on Surface Acoustic Wave (SAW) sensors. The main criterion is that the polymer coating reacts with the chemical agent to produce a refractive index change in the coating, which would be detected by the LPG sensor. With the mulitiplexing capability of the LPG technology multiple coatings can be monitored simultaneously to provide a "chemical signature" of the unknown agent. The provided system can be used to further develop these coatings.

Blank

# REFERENCES

Joint Service Chemical and Biological Defense Program, "FY00-FY01 Overview," 2000, <http://www.acq.osd.mil/cp/cbdovw00.pdf>.

Chemical and Biological Defense Program, "Annual Report to Congress," March 2000, Hill, K.O., Y. Fujii, D.C. Johnson, and B.S. Kawasaki, "Photosensitivity in optical fiber waveguides: application to reflection filter fabrication," *Appl. Phys. Lett.* Vol. 32, No. 10, pp 647-649, 1978.

Vengsarkar, A.M., P.J. Lemaire, J.B. Judkins, V. Bhatia, J.E. Sipe, and T.E. Ergodan, "Long-period fiber gratings as band-rejection filters," *Lightwave Technol.* Vol. 14, 58, 1996.

Qu, X., A. Wirsen, and A.-C. Albertsson, "Novel pH-sensitive Chitosan hydrogels: swelling behavior and states of water (Engl. transl.)," *Polymer* Vol. 41, No. 12, pp 4589-4598, 2000.

DEPARTMENT OF THE ARMY
CDR USASBCCOM
ATTN AMSSB SCI C
5183 BLACKHAWK ROAD
APG MD 21010-5424

OFFICIAL BUSINESS

**FIRST CLASS**